The influence of subaquatic springs in lacustrine sedimentation: origin and paleoenvironmental significance of homogenites in karstic Lake Banyoles (NE Spain)

Mario Morellón*[1, 2], Flavio S. Anselmetti[3, 2], Blas Valero-Garcés[4], Santiago Giralt[5], Daniel Ariztegui[6], Alberto Sáez[7], M. Pilar Mata[8], Fernando Barreiro-Lostres[4], Mayte Rico[4], Ana Moreno[4]

[1] *Instituto de Geociencias (CSIC, UCM),Calle José Antonio Nováis, 2, 3ª planta, 3b. Facultad de Ciencias Geológicas, Univ. Complutense. 28040 Madrid, Spain.*

[2] *Swiss Federal Institute of Aquatic Science and Technology, Eawag, Ueberlandstrasse 133, CH-8600 Dübendorf, Switzerland.*

[3] *Institute of Geological Sciences and Oeschger Centre of Climate Change Research, University of Bern. Baltzerstrasse 1. CH-3012 Bern, Switzerland.*

[4] *Department of Environmental Processes and Global Change. Pyrenean Institute of Ecology (IPE) – CSIC. Campus de Aula Dei. Avda Montañana 1005. E-50059 Zaragoza, Spain.*

[5] *Institute of Earth Sciences Jaume Almera (ICTJA-CSIC). Carrer Lluis Sole i Sabaris s/n. E-08028 Barcelona, Spain.*

[6] *Section of Earth Sciences. University of Geneva. Rue des Maraîchers 13. CH-1205 Genève, Switzerland.*

[7] *Department of Stratigraphy, Paleontology and Marine Geosciences. Universitat de Barcelona. C/ Marti Franques s/n. E-08028 Barcelona, Spain.*

[8] *Instituto Geológico y Minero de España (IGME). C/ Calera 1. E-28760 Tres Cantos (Madrid), Spain.*

*Corresponding author. E-mail address: mario.morellon@igeo.ucm-csic.es

ABSTRACT

Banyoles (42º08'N, 2º45'E) is the largest and deepest lake of karstic-tectonic origin in the Iberian Peninsula. The lake comprises two basins and six sub-circularly shaped sub-basins fed by subaquatic springs. Periods of intense groundwater inflow in the deepest sub-basins lead to the fluidization and re-suspension of previously deposited sediments and subsequent settling forming homogenite deposits on the southern basin intermediate platforms. The multiproxy analysis of sediment cores combined with high resolution seismic stratigraphy (3.5 kHz pinger and multi-frequency Chirp surveys), allows a precise reconstruction of depositional environments and related hydrological variability and groundwater inflow during the last ca. 7.6 cal kyr BP. According to the age model based on ^{137}Cs, ^{210}Pb and AMS ^{14}C dating, homogenite deposition occurred between 7.2 and 5.5 cal kyr BP, stopped during the middle Holocene (5.5 - 2.8 cal kyr BP) and greatly increased during the last two millennia with a total of 17 homogenite layers individually up to 75 cm-thick. The onset of this unique sedimentation mode at ca. 3 cal kyr BP coincides with an increase in lake level, evidenced by the onlapping of fine-grained, distal sediments over coarser massive, carbonate-rich, littoral deposits. A detailed, multidisciplinary study of the homogenites (sedimentology, physical properties, high-resolution elemental geochemistry, mineral composition, grain-size, organic matter content and SEM) combined with seismic stratigraphy demonstrates that the fluidization events triggering the formation of the homogenites were caused by higher and more intense local groundwater inflow, related to increased rainfall during the Late Holocene and likely intensified by land use changes during the last millennium.

Keywords: karstic lake, subaquatic springs, groundwater, turbidity plumes, homogenites, Holocene

1. Introduction

Groundwater constitutes an essential hydrological resource in Mediterranean areas characterized by a summer drought period and frequent negative hydrological balance phases, which are particularly threatened by global change (Younger et al., 2002a; García-Ruiz et al., 2011). In these regions, aquifers are essential for sustaining human activities and limnic ecosystems (Edmunds et al., 2004; Álvarez-Cobelas et al., 2005; Shapley et al., 2005). The groundwater input to the hydrological balance is rarely quantified in most lakes, however, subaquatic springs are commonly identified as a significant source for groundwater in lake systems (Canals et al., 1990; Colomer et al., 2002; Assayag et al., 2008; Matter et al., 2010). Recently, such springs and associated pockmarks have been described and imaged thanks to high-resolution geophysical and limnological surveys (e.g., Lake Ohrid, Matter et al., 2010; Lake Kivu, Ross et al., 2014). In spite of their variable relative importance in the hydrological balance of these systems, subaquatic springs commonly supply cool and oxygenated waters, rich in ions and nutrients, leading to the establishment of particular subenvironments and specific habitats for endemic species within lake systems (Matter et al., 2010; Descy et al., 2012a).

Ecological and limnological responses to subaquatic springs are well-studied (e.g., Dead Sea (Ionescu et al., 2012), Lake Bogoria (Dadheech et al., 2013), Lake Kivu (Descy et al., 2012b)) and extensive research has been carried out on associated carbonate sedimentary features (i.e., microbialites, teepee structures, diagenetic iron-rich shoreline indicators and carbonate crusts) (Warren, 1982; Burne and Moore, 1987; Winter, 1999; Rosen et al., 2002, 2004). However, less attention has been paid to the physical effects of groundwater input in sedimentation and its potential to remobilize significant amounts of sediments (Bloesch, 1995; Draganits and Janda, 2003). Examples of fluidization and resuspension of offshore lake sediments and consequent re-deposition of thick ‘homogeneous’ layers, termed homogenites,

have been exclusively described as a result of shaking and/or subaqueous mass-wasting slope processes caused by earthquakes (Beck, 2009). However, intense and focused groundwater input through subaquatic springs could be also able to produce a similar effect in sedimentation, not yet described in detail in lake settings. Although these groundwater-fed lake basins often provide long, continuous sequences with high temporal resolutions, suitable for palaeohydrological and palaeoclimate reconstructions (Morellón et al., 2009; Valero-Garcés et al., 2014), an adequate understanding of sedimentary processes is essential to reconstruct the evolution of groundwater inputs, their impact in lake sedimentation and their role in homogenite formation (Shapley et al., 2005).

Lake Banyoles (NE Spain) belongs to a groundwater-fed karstic system and constitutes a unique example in the Iberian Peninsula of offshore sedimentation partly controlled by the activity of subaqueous springs. Geophysical and limnological surveys during the last decades have documented the resuspension and fluidization of sediments by focused groundwater inflow at the deepest sub-basins of the lake (Canals et al., 1990; Casamitjana and Roget, 1993), leading to the development of turbidity plumes (Serra et al., 2005). These 'fluidization events' have been related with episodes of intense rainfall in the recharge area of the aquifer feeding the lake (Soler et al., 2007, 2009). Although Banyoles has been extensively investigated from a limnological point of view, the impact of groundwater dynamics on the sediments across the lake, and the spatial and temporal extent of this impact at longer timescales than the last few decades, remains unknown. Moreover, the depositional history of the lake has been exclusively studied at the littoral areas of the sedimentary basin (Pérez-Obiol and Julià, 1994; Valero-Garcés et al., 1998; Cho Martínez, 2012; Höbig et al., 2012) and at emerged pre-Holocene paleolake deposits (Julià-Brugués, 1977; Leroy, 1990, 1997, 2008; Løvlie and Leroy, 1995), where first evidence of massive, homogeneous sediment deposits related to the activity of underwater springs was described (Leroy, 1990, 2008).

However, these deposits were not investigated in detail from a sedimentological point of view.

This paper aims to fill this gap in the investigations carried out in Banyoles and provides a Holocene sedimentary reconstruction using offshore sediments with special emphasis on sedimentary processes associated with fluidization events related to higher groundwater input episodes through subaquatic springs. The combined use of high-resolution seismic stratigraphy and a multi-proxy analysis of sediment cores recovered at distal areas of the lake enable a precise reconstruction of the spatial extent, timing and different intensity of groundwater discharge. The associated sedimentary processes are evaluated in relation to climate variability and changes in land use during the last millennia.

2. Regional setting

2.1 Geological and geomorphological setting

Lake Banyoles (42º1'N; 2º4'E, 173 m a.s.l.), located in the NE margin of the Iberian Peninsula, 20 km west of the Mediterranean Sea (Fig. 1A), lies in a tectonic-karstic basin (Julià, 1980) and is formed by several cone-like karstic depressions (Fig. 1B). The lake is located in the eastern South-Pyrenean Foreland Basin (Burbank et al., 1992; Bischoff et al., 1994) affected by widespread Neogene extension (Saula et al., 1994; Tassone et al., 1994). The bedrock comprises the mid Eocene Banyoles Formation, mainly composed of marine, organic- and pyrite-rich marls and mudstones, underlain by the Eocene Beuda Formation consisting of massive gypsum (200-300 m), and the 100 to 200 m thick Perafita Formation dolostones (Barnolas, 1992; Mató i Palós et al., 1996; Serra-Kiel et al., 2003). The contact between these last two formations has led to a bedrock 'de-dolomitization' process due to gypsum dissolution, a particularly intense karstification mechanism responsible for the formation and collapse of the Lake Banyoles depressions (Bischoff et al., 1994). Karstic

128 processes (e.g., collapse depressions, intermittent springs, karren fields) are still active in the
129 lake catchment (Julià, 1980; Sanz, 1981; Canals et al., 1990), as demonstrated by the
130 12/11/1978 collapse, when a new sub-basin ('Estanyol Nou') was formed near to the
131 southwestern shore (Höbig et al., 2012), or the 1989 collapse of the road 150 to 200 m north
132 of Lake Banyoles, by normal concentric faults at Can Guixeres (Leroy, 1997).

133 Lake Banyoles is the last remnant of a larger lacustrine basin developed during
134 Pliocene-Quaternary times, known as the Banyoles-Besalú system, which occupied 90 km^2
135 (Julià-Brugués, 1977; Canals et al., 1990). Travertine formations and calcareous lithologies
136 are common, both in ancient terraces (Julia Bruguès and Suc, 1980; Leroy, 1997, 2008) and
137 present lacustrine deposits (Coma et al., 1987, 1988). The age of the travertine formation
138 damming the eastern margin of the modern lake is ~120 to 45 kyr BP (Julià and Bischoff,
139 1991), which represents the potential maximum age of the lacustrine deposits accumulated
140 within the basin.

141 The littoral zone of the modern lake (0-3 m water depth) is covered by a thin
142 macrophyte vegetation belt of *Phragmites, Schoenoplectus* and *Myriophyllum*. Sediments
143 range from travertines and calcareous sands in the littoral areas, to carbonate-rich silts and
144 clays in the distal areas (Rieradevall and Roca, 1995).

145

146 *2.2 Morphometry, hydrology and limnology of the lake*

147 The lake has a N-S elongated shape and a surface of 118 ha. The lake is formed by 6
148 main circular-shaped sub-basins (B1 to B6), with steep margins and water depths ranging
149 from 7.5 to 44 m, connected by shallower, flat platforms (ca. 20 m and 5-10 m water depths in
150 the southern and northern areas, respectively) (Moreno-Amich and García-Berthou, 1989;
151 Canals et al., 1990) (Fig. 1B). Karstic depressions confer a lobed shape to the lake shoreline,

and a shallow (< 12 m maximum water depth) and narrow (< 500 m) sill in the center divides the lake into two basins, here referred as northern and southern ones (Fig. 1B).

The lake is hydrologically open and mainly groundwater-fed through subaquatic springs located in the deepest sub-basins of the southern basin (B1 and B2) (Moreno-Amich and García-Berthou, 1989; Canals et al., 1990). Surface water input derived from the 11.42 km^2 catchment drained by the creeks located in the western area of the lake has been quantified as 100 to 300 l/s for May-September 1984, whereas output through the canals at the eastern margin (Fig. 1C) ranges from 568 to 1080 l/s for the same period (Dutras et al., 1986; Canals et al., 1990). Thus, groundwater supplies 85% of the total water input (Casamitjana et al., 2006). Lake water in southern basin is characterized by a lower residence time and higher oxygenation levels than water in the northern lobe. Particularly, sub-basin B1 provides 90% of groundwater input (Serra et al., 2005). The other main sub-basins of the northern basin (Fig. 1B) have a lower groundwater input so that anoxic conditions and sulfide production at the hypolimnion occur (Guerrero et al., 1978; Garcia-Gil et al., 1993). Thus, the 6 sub-basins are connected by their epilimnetic waters, but their respective hypolimnions are isolated and show different anoxic periods, ranging from 1 to 12 months/year (Prat and Rieradevall, 1995).

Surface lake waters are sulphate and calcium-rich ($[SO_4^{2-}] > [HCO_3^{2-}] > [Ca^{2+}] > [Mg^{2+}]$) (Bischoff et al., 1994), with an electrical conductivity of 1300 to 1400 µs/cm and a pH between 7 and 8.1 (MAGRAMA, 2006). Water temperature ranges from 8 to 25 °C depending on the water depth and season (Rieradevall and Roca, 1995). Oxygenation conditions are also spatially variable and depending of groundwater input, ranging from oxic (0-7 m water depth), to one month of anoxia (sub-basin B1, >12 m water depth), and to long-lasting anoxia (sub-basins B3 and B4, >12 m) (Rieradevall and Roca, 1995). The lake is monomictic, with water stratification from April to October. A chemocline is also present in

177 sub-basins B1 and B4 at 19-20 and 13-17 m water depth respectively, which leads to long
178 anoxic periods in the hypolimnion (Rieradevall and Roca, 1995).

179 Differences in the thermal inertia and incoming flux through the subaqueuous springs,
180 located in the northern and southern basins, move denser water during the winter season from
181 the shallower northern to the deeper southern basin. This leads to a bottom current with a flow
182 of 20000 l/s and a velocity of up 12 cm/s that redistributes water between the two basins,
183 replacing northern basin waters every ~5 days. This exchange constitutes the main current
184 dominating circulation in the lake (Roget et al., 1993; Casamitjana et al., 2006).

185

186 *2.3 Groundwater and turbidity plumes*

187 The lake constitutes a 'trop-plein' of a complex aquifer system whose recharge area is
188 located in the Alta Garrotxa Range, 15 to 40 km northwards (Sanz, 1981; Brusi et al., 1990).
189 The NE-SW trending Albanyà fault, east of the lake, constitutes a subvertical dam for the
190 groundwater (Moreno-Amich and García-Berthou, 1989). Most of the deepest sub-basins (B1,
191 B2, B4, B5 and B6) are filled with several meters of sediments maintained in suspension by
192 the intense groundwater inflows forming a sharp and horizontal upper sediment interface,
193 known as the lutocline which is recognizable in seismic profiles (Canals et al., 1990) (Fig.
194 1D). These suspensions have particle concentrations varying from 0.18 to $< 10^{-3}$ g/l and rather
195 constant temperatures (~19ºC) (Casamitjana et al., 2006). According to geophysical surveys
196 and sedimentological analyses, sediments in sub-basins B1, B3 and B4 appear as 'mobile'
197 particles in suspension, whereas they are usually denser and more consolidated in B2,
198 resulting in an acoustic bedding at the bottom of this sub-basin (Colomer et al., 2002). The
199 momentum of the underground spring and sediment grain-size determines the maximum
200 height that the lutocline can rise to in each case (Casamitjana et al., 1996; Colomer et al.,

1998). Fluctuations of the lutocline depths in B1, B3 and B4 are comparatively smaller than B2 and show simultaneous shifts (Casamitjana and Roget, 1993).

Most intense fluidization and re-suspension processes, and associated hydrothermal plumes, are restricted to the deepest sub-basins B1 and B2. Sub-basin B1 is fed by the largest groundwater flow (~500 l/s). Its sediment fill has a vertical thickness of 45 to 50 m and a sediment density of 100 to 130 g/l (Colomer et al., 2002). Its lutocline oscillates from 29.2 to 32.0 m water depth (Serra et al., 2005) (Fig. 1D). In contrast, B2 has a sediment fill with maximum vertical thickness of 32 m and experiences periodic large fluctuations in sediment density from 280 to 180 g/l and larger lutocline migrations (from 25 to 45 m). Sediment fluidization processes occurs episodically associated with particular intense rainfall events in the aquifer recharge area (average monthly values 1.5 to 4.5 times larger than the long term mean, 1970-1999) (Colomer et al., 2002). Thus, sub-basin B2 acts as an overflow of the groundwater system.

Due to the difference between temperature of the lutocline and the hypolimnetic water immediately above B1, an upward-directed permanent hydrothermal plume develops (Colomer et al., 2001). This plume carries a suspension of particles from the lutocline up to a maximum height, which varies depending on the stratification depth of the water column. During the mixing period, this plume reaches the surface of the lake, spreading laterally and forming a ~7 m-thick turbidity current, with a sediment concentration of ~0.01 g/l (Serra et al., 2002, 2005). According to sediment-trap studies, particle fluxes oscillate from 10 to 25 g m^{-2} day^{-1} near to B1 to < 5 g m^{-2} day^{-1} in more distant areas of the southern basin (Serra et al., 2002, 2005).

An additional temporal, hydrothermal turbidity plume develops above sub-basin B2 due to fluidization events after intense rainfall in the aquifer recharge area (Soler et al., 2009). The onset of the fluidization is characterized by episodic groundwater influx entering through

preferential paths in the more consolidated sediment at the bottom of sub-basin B2. The water pressure through small diameter conduits within the sediment causes a high mean upward velocity, which is three orders of magnitude greater than in perennial plume B1. After such an event, water-flux velocity decreases progressively and resuspends the settled sediment. Finally, when sediments are totally fluidized, the episodic hydrothermal plume of sub-basin B2 resembles that of the perennial plume of B1 (Soler et al., 2009). When the hydrothermal plume in sub-basin B2 is fully developed, a large quantity of sediment is transported upwards from the lutocline, resulting in an increase in sedimentation rates in the southern basin (ca. 156 g m^{-2} day^{-1}), which is one order of magnitude higher than in periods without fluidization, when only the B1 hydrothermal plume remains active (Serra et al., 2002; Casamitjana et al., 2006; Soler et al., 2009).

As the two basins of the lake (N and S) are separated by a shallow sill (Fig. 1B), sediments transported by turbidity plumes are restricted during the stratification period to the southern basin. In contrast, during the mixing period, particles can reach the surface of the lake, spreading laterally and subsequently settling across the entire lake bottom (Soler et al., 2009). However, sedimentation in the northern basin is not significantly affected by re-suspended sediments and carbonate-rich silts and sands with abundant encrusted charophyte stems and other calcitic bioclasts (e.g., ostracods, gastropods) are predominant (Serra et al., 2005). Thus, the effect of turbidity plumes on sedimentation is mostly restricted to the southern basin.

3. Materials and methods

A geophysical survey was carried out in April 2011 using a high-resolution, single-channel seismic system with a centre frequency of 3.5 kHz (GeoAcoustic pinger source) and a EdgeTech Chirp 3100-P multi-frequency profiler, covering 22 km and 14 km of seismic lines,

respectively. This dense grid consisting of ~36 km of seismic lines provides a mean spatial resolution of ~100 m between each line (Fig. 1C). Seismic processing workshop software was used for the processing of the pinger data (bandpass filter, flat gain) and the resulting seismic data set was interpreted using the Kingdom Suite software.

In May 2011, three pairs of overlapping sediment cores (BAN-11-1A, 2A and 3A) with maximum lengths of ~13, 12 and 5 m, respectively, were recovered using an Uwitec© percussion coring equipment installed on a floating raft. This research focuses on core 1A, recovered in the flat platform between sub-basins B1 and B2, at ca. 21 m water depth. Additional coring sites 2A and 3A are located in the northernmost area of the lake and sub-basin B3, respectively. Three short, gravity cores were obtained to recover the uppermost part and the sediment/water interface of the three sequences. Seven additional short cores (BAN-12-1, 2, 3, 4, 5, 6 and 8) were recovered in July 2012 along a transect between B1, B2 and the location of the longest core BAN-11-1A (Fig. 1C). Cores recovering suspended sediments of sub-basins B1 and B2 (BAN-12-1 and 2) were maintained in upright position until sediments were stable and settled down, before excess water was eliminated. The uppermost 60 cm of the BAN-11-1A sequence was sub-sampled in the field every 1 cm for ^{137}Cs and ^{210}Pb dating.

Physical properties (magnetic susceptibility, gamma density, P-wave velocity) were measured in core BAN-11-1A with a Geotek Multi-Sensor Core Logger (MSCL) every 1 cm. All the cores were subsequently split in two halves and imaged with a digital camera. The Lightness (L*) parameter was obtained from the core pictures using Adobe Photoshop CS and Image J software. Lithotypes were defined after visual and microscopic smear slides observation, applying the methodology described in Schnurrenberger et al. (2003) (Table 1).

Elemental composition of core BAN-11-1A sediments was obtained by using an AVAATECH XRF core scanner at a resolution of 5 mm and under two different working conditions: i) with an X-ray current of 0.8 mA, at 10 s count time and 10 kV X-ray voltage for

276 the measurement of Al, Si, P, S, Cl, Ar, K, Ca, Ti, V, Cr, Mn and Fe; and ii) with an X-ray
277 current of 2 mA, at 30 s count time and 30 kV X-ray voltage for the measurement of Ni, Cu,
278 Zn, Ga, Ge, As, Se, Br, Rb, Sr, Y, Zr, Nb, Au, Pb, Th and U. The XRF results are expressed
279 as counts per second (cps) and only chemical elements with mean cps over 1500 were
280 considered to be statistically significant.

281 Grain size of short cores BAN-12-1 and 2 was measured every 4 cm. Core BAN-11-
282 1A was measured at variable resolutions: for grain size: ~8 cm at the uppermost 610 cm and
283 ~25 cm at the lowermost part of the sequence, for TOC and TIC every 3 cm, and for X-ray
284 diffraction every 9 cm. Grain size was determined using a Malvern Mastersizer 2000.
285 Samples were pre-treated with 15% hydrogen peroxide on a hot plate at 80°C to eliminate the
286 organic matter; a dispersant agent and ultrasound treatment were used prior to measurement.
287 Total organic carbon (TOC) and total inorganic carbon (TIC) were measured with a LECO
288 SC 144 DR elemental analyzer. Whole sediment mineralogy was characterized by X-ray
289 diffraction with a Bruker-AXS D5005 (working conditions: Cu kα, 40 kV, 30 mA and
290 graphite monochromator) and relative mineral abundance was determined using peak
291 intensity following the procedures described in (Chung, 1974a, b). Results are expressed in
292 percentages with respect of the total dry weight of the sample.

293 Scanning electron microscope images were taken of dried sediment samples of cores
294 BAN-11-1A, BAN-12-1 and -2 under low-vacuum conditions in an environmental scanning
295 electron microscope FEI Inspect on uncoated fragmented samples. Backscattered electron
296 (BSE) images were obtained in order to detect compositional differences of the components
297 as grey level contrast. In addition, energy dispersive X-ray spectrometry (EDS) analysis was
298 performed when necessary.

299 The chronology of the lake sequence is based on: i) 9 accelerator mass spectrometry
300 (AMS) ^{14}C dates from core BAN-11-1A, analyzed at the ETH-Zürich Laboratory of Ion Beam

Physics and at DirectAMS radiocarbon services (Seattle, USA) (Table 2) and on ii) ^{137}Cs and ^{210}Pb dating by gamma spectroscopy at Eawag (Dübendorf, Switzerland). Excess (unsupported) ^{210}Pb was calculated as difference between total ^{210}Pb and ^{226}Ra for individual samples. Corrected radiocarbon dates were converted into calendar years BP with Calib 6.0 software using the INTCAL 09 calibration curve (Reimer et al., 2009), selecting the median of the 95.4% distribution (2σ probability interval) (Table 2). The age-depth relationship was constructed by linear interpolation of the 1963 AD ^{137}Cs maximum activity peak and calibrated radiocarbon dates using Analyseries (Paillard et al., 1996).

4. Results

4.1 Seismic Stratigraphy

In spite of frequent gas masking throughout the lake basin, particularly in the northern basin, locally high penetration into the sub-surface down to the acoustic basement allowed tracking of the bedrock morphology in many parts of the lake. Maximum seismic penetration reached up to 20 m in the northern basin of the lake (Fig. 1D), and 18 m in the southern basin (Fig. 2), where substratum was not reached. These two basins —separated by a shallow sill with no seismic penetration (Fig. 1D)— show a different seismic stratigraphy due to their complex bathymetry and variable sedimentological processes. The southern basin is characterized by the flat bottom areas in B1 and B2 (Fig. 1B, D), corresponding to the lutoclines (Canals et al., 1990), and extensive and rather flat areas at ~20 m water depth between and around these two main depressions, displaying moderate seismic penetration (Fig. 2). The bedrock surface was identified in a previous lower-frequency survey (150-2000 kHz) (Canals et al., 1990) and is characterized by local irregularities and discrete steps and sharp edges, consistent with the karstic origin and active dynamics of the two depressions.

Seismic stratigraphic analysis of our 3.5 kHz survey allowed the identification of three major seismic units (SA-SC; Fig. 2) and several seismic horizons, which have been tracked through the southern basin. These horizons and units were correlated with the core lithostratigraphy (see below). A constant acoustic velocity of 1500 m/sec based on the MSCL measurements has been used for the seismic-to-core correlation (Fig. 2A).

The oldest seismic unit (*Unit SA*) reaches more than 10 m thickness and is only recognizable in areas located close to the eastern lake margin. It is characterized by rather continuous, mid-amplitude reflections and intercalated seismically more transparent units up to 2 m thick. The lowermost part of core BAN-11-1A reached the uppermost part of this seismic unit (Fig. 2A).

Unit SB is visible only in few areas and consists of continuous low-amplitude reflections with the intercalation of two higher amplitude reflections, coinciding with rather homogeneous lithology (Fig. 2A).

The youngest seismic unit *(Unit SC)* has been mapped through larger areas of the southern basin and reaches ~10 m in thickness in the central areas of the platforms. Seismic facies are characterized by the alternation of high-amplitude, laterally continuous reflections and transparent layers, slightly increasing basinward in thickness up to ~1 m thick (Fig. 2). The upper part of this seismic unit onlaps over SA and SB units and corresponds in sediment core BAN-11-1A with a lithological change to sediments with higher and more variable density (Fig. 2A).

4.2 Sedimentology

4.2.1 Lithotypes and core stratigraphy

Six lithotypes have been defined in the long (BAN-11-1A) and short (BAN-12-1 to 8) sediment cores recovered from the southern areas of Lake Banyoles, on the basis of detailed

sedimentological descriptions, smear-slide and SEM microscopic observations and compositional analyses. According to textural and compositional criteria, these lithotypes have been grouped into two main categories: i) banded to laminated and ii) massive (Table 1, Figs. 2-4).

Banded and laminated lithotypes (Fig. 4A-C) are composed of variable amounts of: i) mud-size (10-15 μm) elongated low magnesium calcite (LMC) crystals derived from direct precipitation from lake waters (Fig. 5B), ii) reworked biogenic particles from the littoral areas (*Chara* fragments, micrite oncoids, ostracods and gastropod fragments of different sizes (<50 μm)); iii) diatoms and other organic components (Fig. 5A, C); and iv) detrital particles, including carbonates, quartz grains and clay minerals (mainly illite and chlorite) derived from the weathering and erosion of the soils and bedrock in the watershed (Figs. 3, 5A). Grain-size distribution is dominated by the silt fraction, with mean values ranging from 5 (lithotype 1) to ~20 μm (lithotype 3) (Table 1, Fig. 3).

Massive lithotypes (Fig. 4D- F) occur as: i) up to 120 cm thick, fining upwards sequences, ranging from carbonate-rich sands (lithotype 6, ~65 μm mean grain size) to fine-grained silts (lithotype 5, ~10 μm mean grain size), capped by clay-sized particles at the top. These sediments are more carbonate-rich than banded and laminated lithotypes (Fig. 3) and contain higher amounts of coarse and fine-grained particles (from sands to silts) of reworked components (fragmented bioclasts, sub-rounded grains) (Fig. 5D-F). They are restricted to the lowermost part of the recovered succession and deposited by turbidity currents caused by the collapse of littoral areas (mass-wasting deposits) (Figs. 3, 4F)

ii) ‘homogenites’ (lithotype 4) occurring as 2 to ~75 cm-thick layers lacking any clear vertical grain-size distribution, composed of poorly sorted, fine-grained silts with mean sizes ranging from 6 to 12 μm (Figs. 3, 4E). These layers are likely deposited after the fluidization of sediment particles maintained in suspension at the deepest sub-basins of the lake (B1 and B2)

375 and they are more abundant in the upper part of the sequence. They are described in detail
376 below.
377 According to their lithology (Table 1, Fig. 3), the sedimentary succession in the southern
378 basin of Lake Banyoles has been divided into three main lithological units (LA, LB, LC)
379 matching with facies associations.
380 *Unit LA* (1298 to 970 cm core depth) is characterized by the presence of carbonate-
381 rich, silty lithotype 3 at the base (Figs. 3, 4C), leading to an alternation between more, fine-
382 grained lithotype 1 and relatively thin beds of massive lithotype 4 at in the middle of this unit.
383 A thick mass-wasting deposit (~120 cm), with a sandy layer at the base (lithotype 6) and
384 massive lithotype 5 occurs in the uppermost part of this interval (Figs. 3, 4F). This unit
385 represents the transition from a relatively shallow, carbonate producing depositional
386 environment with bioturbation and thus, oxic conditions (lithotype 3) to a relatively deeper
387 setting (lithotype 1) accompanied by intensification of groundwater inflow (lithotype 4) and
388 mass-wasting activity (lithotype 6).
389 *Unit LB* (972 to 610 cm core depth) is characterized by the deposition of carbonate-
390 rich, silty lithotype 3 (Figs. 3, 4C, Table 1), interbedding mm-thick layers of massive silts.
391 This unit deposited in a shallow, carbonate producing, oxic depositional environments with
392 abundant littoral fauna and variable detrital input.
393 *Unit LC* (610 to 0 cm core depth) starts with the deposition of banded to laminated
394 lithotype 2, reflecting more oxygen-depleted conditions associated with more distal/offshore
395 deeper depositional environments than Unit LB (Figs. 3, 4B, Table 1). Upcore, sediments are
396 composed by an alternation of cm-thick fine-grained sediments interval (lithotype 1) and thick
397 layers of homogenites (lithotype 4) (Fig. 4D, E). This unit represents dominant distal
398 deposition at the coring site away from the slope of the margin of the lake, with relatively low
399 oxygenation conditions. The succession of lithotypes 3, 2 and 1 suggests a progressive

400 increase in lake level, confirmed by the seismic onlapping of unit C onto B (Fig. 2). The
401 deposition of up to 17 homogenite layers, with a maximum thickness of ~75 cm, also reflects
402 an abrupt intensification of groundwater activity during unit LC. The decrease in frequency
403 and thickness of lithotype 4 layers in the uppermost part of the succession is interpreted as a
404 decrease in groundwater activity in more recent times, accompanied by increased carbonate
405 and organic content (Figs. 3, 6A).
406
407 *4. 3 Seismic to core correlation and depositional evolution*
408 Seismic to core correlation enables a basin-wide reconstruction of the main stages in
409 the Holocene depositional history of Lake Banyoles (Fig. 2A).
410 On the basis of seismic facies and the alternation of density contrasts, seismic Unit SA
411 is interpreted as a sedimentary succession characterized by the intercalation of massive
412 lithotypes (4, 5 and 6) within a sequence from distal-fine grained lithotype 1 to littoral
413 carbonate-rich lithotype 3 (Figs. 2A, 3). Deposition of mass-wasting deposits and turbidites –
414 as the one > 1 m thick turbidite (lithotypes 5 and 6) at the top of this unit - could have been
415 more frequent during an early stage of development of the southern basin depressions with
416 more active karstic collapses. Additionally, several relatively thin (up to 25 cm-thick)
417 homogenites (lithotypes 4 and 5) also occur at the lowermost part of this unit (Figs. 2A, 3).
418 According to lithology, low-amplitude reflections with the intercalation of two higher
419 amplitude reflections in SB are interpreted as the dominance of acoustically homogeneous,
420 carbonate-rich lithotype 3 deposits with frequent clastic intercalations. A basinward increase
421 in thickness (from ~4 m in coring location to more than 6 m in more distal areas) might be
422 related to the occurrence of mass-wasting deposits at the lower part of the recovered sequence
423 (Fig. 2).

Finally, seismic facies observed in uppermost unit SC correspond to the alternation between lithotype 1 and thick homogeneous lithotype 4 layers, characterized by higher and constant density values (Fig. 2A). The onlapping of this unit above lowermost ones (A, B) suggest an increase of lake level associated with the deposition of more fine and distal lithotypes 1 and 4; higher groundwater flow (main water source of Lake Banyoles) is likely associated with these periods of higher lake level. Good lateral continuity of reflections and thickening of seismically transparent units towards the deepest sub-basin B2 suggests that the origin of homogeneous lithotype 4 is related to depositional processes around this sub-basin (Fig. 2).

4.4 Age model

To construct the age model, a total of 9 radiocarbon dates from core BAN-11-1A (Table 2) was used. Most of the dated samples correspond to bulk organic matter due to the absence of terrestrial organic macroremains. A large reservoir effect is suspected as recent sediments (44.5 cm depth) yielded an uncorrected age of 5460 ± 35 ^{14}C yr BP. To determine this reservoir effect and their likely variability through time, we used two couples of dates, each of them from the same stratigraphic levels: i) at the top of the sequence, characterized by sedimentation under relatively deep conditions, similar to present-day (lithotypes 1 and 4), comparing ^{137}Cs maximum activity peak of 1963 AD and a radiocarbon date on bulk organic matter (reservoir effect = ~5470 yrs); and ii) at the base of the core, with predominantly shallow-water conditions (lithotype 3), comparing two radiocarbon dates derived from a terrestrial macro-remain (charcoal) and bulk organic matter (reservoir effect = ~3025 years) (Table 2).

The estimated reservoir effects for the top and the base of the core were subtracted from radiocarbon dates made on bulk organic matter at lithological units LC and LA-LB,

449 respectively. A consistent result was obtained in lowermost units A and B, with a rather
450 constant sedimentation rate of ~0.1 cm / year (Fig. 7A). The comparatively higher reservoir
451 effect obtained for the uppermost unit C, characterized by higher lake levels, might be
452 explained by higher input of dissolved carbon from groundwater, likely higher during this
453 recent stage. Variations in groundwater flow and potential reworking of organic particles from
454 the deepest sub-basins B1 and B2 might also be responsible for the radiocarbon reversals
455 occurring within unit A. Thus, the three radiocarbon dates of units A and B were considered
456 for the chronology of the sequence, while all the other dates were rejected (Table 2, Fig. 7A).
457 Corrected dates were calibrated into calendar years and the age-depth relationship was
458 constructed by linear interpolation (Fig. 7A). Event layers, deposited instantaneously and
459 represented by massive lithotypes 4, 5 and 6 (i.e., homogenites in lithological units LA and
460 LC (Fig. 7A, B) and the mass-wasting deposit at the top of unit A), were subtracted from the
461 age model. According to this, the Lake Banyoles sequence spans the last ~7600 cal years BP.
462 The uppermost unit LC was deposited during the last ~2800 cal years. The age-depth
463 relationship shows an abrupt increase of sedimentation rate at the transition between units LB
464 and LC, from 0.1 cm / year to 0.23 cm / year, including event layers (Fig. 7A). The abundance
465 of these homogenites in the upper unit explains this sedimentary rate change (Fig. 7B). The
466 internal chronology for the uppermost unit, between the uppermost validated date (~2800 cal
467 yrs BP) and the 1963 AD maximum ^{137}Cs activity peak, remains unclear due to the lack of
468 dates. Three different models can be used as an approximation: model 1) an extrapolation of
469 ^{137}Cs inferred sedimentation rate throughout the interval containing the homogenites; model
470 2) an interpolation between ^{137}Cs peak and valid date (2800 cal yrs BP) at the uppermost part
471 of unit B; and model 3) an interpolation between ^{137}Cs peak and lowermost (not valid)
472 radiocarbon date of unit C. According to these different age models, the occurrence of

473 homogenites could be restricted to the periods 1840-1938 AD, 380-1600 AD or 1340-1720
474 AD, respectively (Fig. 7B).
475
476 *4.5 Sedimentological and geochemical characterization of homogenites*
477 Lithotype 4 is dominant throughout the uppermost part of the sequence (lithological
478 unit LC) (Figs. 3, 6A) and is also present occasionally at the lowermost unit LA, recovered in
479 the platform between deepest sub-basins B1 and B2. These intervals are defined by their
480 regular colour, texture and composition, with minor or no internal variations. Compared to
481 intercalated lithotype 1, they are characterized by a lighter colour (higher L* values, > 60),
482 higher magnetic susceptibility (MS), higher density and a slightly coarser grain size, as
483 evidenced by higher mode (~6 μm) and mean values (6 to 12 μm) (Figs. 3, 4E, 6A).
484 These homogenites are also characterized by a slightly higher organic and carbonate
485 content (as recorded by TIC, calcite and higher Ca and Sr values) (Figs. 3, 6A). Consequently,
486 they have a relatively lower concentration of siliciclastic minerals (quartz and clay minerals)
487 and elements associated with this fraction (Al, Si, K, Ti, Zr, Fe, Mn) as summarized by lower
488 Ti/Ca values (Fig. 6B). Other geochemical properties characterizing lithotype 4 are: i) a lower
489 Sr/Ca ratio, likely revealing a lower proportion of aragonite, common in biogenic particles
490 mostly reworked from littoral, carbonate-producing areas of the lake; ii) higher S values; and
491 iii) a higher Fe/Mn ratio, likely indicating more local anoxic conditions during the deposition
492 of these layers (Fig. 6A).
493 Detailed inspection of SEM images supports previous textural and compositional analyses
494 (Fig. 3) and reveal: i) slightly coarser grain size in homogenites than facies 1 (Fig. 5A, D), ii)
495 more evidence of transport and reworking in homogenites (broken diatoms, irregularly shaped
496 grains, etc.) (Fig. 5 D-F), iii) a higher content of well-developed, endogenic and regular
497 calcite crystals in lithotype 1 (Fig. 5B), iv) a higher content of pyrite framboids in

498 homogenites likely related to higher S concentrations (Fig. 5E) and v) the exclusive presence
499 of the most fragile terrestrial components (e.g., plant remains) in offshore/distal deposits of
500 lithotype 1 (Fig. 5C). Moreover, reworked planktonic calcareous algae remains exclusively
501 occur in the homogenites of lithotype 4 (Fig. 5E).

502 Suspended sediments recovered below the lutoclines of the deepest sub-basins B1 and B2
503 show a very similar sedimentary features compared to homogenites, characterized by light
504 grey colours (slightly reddish in B1 and bluyish in B2) (Fig. 4G, H). Both homogenites and
505 sediments from these sub-basins are, when compared with offshore/distal lithotype 1,
506 characterized by higher carbonate content as reflected by higher Ca/Ti ratios (Fig. 6B).
507 Average mean grain sizes in B1 (core BAN-12-2) and B2 (core BAN-12-1) average 8.6 and
508 9.6 μm, respectively, slightly coarser than in the homogenites (6.5 μm).

509

510 **5. Discussion**

511 *5.1 Homogenites and fluidization events*

512 Textural and compositional analyses of lithotype 4 deposits show a strong
513 homogeneity along the whole layer, particularly visible within uppermost unit LC (Figs. 3,
514 6A). Good lateral correlation of these 'homogenites' between long and short cores (Fig. 8)
515 and inspection of seismic lines (Fig. 2) show that these deposits, absent in the northern basin
516 of Lake Banyoles, appear clearly 'thinning' towards the edges of the southern basin and
517 'ponding' offshore towards deepest sub-basins B1 and B2 (Figs. 2, 8). These layers are
518 characterized by transparent seismic facies with no significant lateral changes (Fig. 2). The
519 origin of homogenites is usually attributed to allochthonous (i.e., distal part of a turbidite)
520 initiated by a mass-wasting process in littoral areas turning into hyperpycnal (turbidity
521 currents with bedload and suspended load) or autochthonous sources (liquefaction,
522 resuspension) (Beck, 2009).

523 Turbidites are usually characterized by single, fining upwards sequences (Hsü and
524 Kelts, 1985; Schnellmann et al., 2005; Girardclos et al., 2007). However, in Banyoles, only
525 the homogeneous layer located at the top of lithological unit LA displays these particular
526 sedimentological features (Figs. 2A, 3, 4F) and thus, is interpreted as a turbidite deposit likely
527 triggered by a mass-wasting episode. On the other hand, considering the location of core
528 BAN-11-1A, less than 100 m from the lake shore, the presence of coarser grain particles at
529 the base of these deposits would be also expected if the area source was the littoral zone of the
530 lake, as described in other similar karstic lakes in the Iberian Peninsula (Morellón et al., 2009;
531 Valero-Garcés et al., 2014).

532 In contrast to turbidite deposition, formation of homogenites in upper unit C involves
533 liquefaction in the deeper sinkholes, resuspension of sediments and vertical transport and
534 settling of the particles in the platform areas. In fact, these mechanisms of transport and
535 deposition have been described for most of the deep sub-basins of the lake, with particular
536 intensity for sub-basins B1 and B2 as a result of intense groundwater inflow (Serra et al.,
537 2002; Soler et al., 2009). Fluidization and resuspension processes in lake sediments can also
538 result from shaking caused by earthquakes. However, this process should be rejected since
539 this region has a low to moderate seismic activity related to some Pyrenean Range faults and
540 only a few earthquakes have been described (Secanell et al., 2004). The only relatively intense
541 (M_w = 6.5) earthquake recorded during historical times occurred in 1427 AD, with the
542 epicenter located ~22 km SW to the lake (Olivera et al., 2006) and likely caused shaking in
543 the lake basin. Nevertheless, given the low frequency of intense earthquakes and the high
544 frequency of homogenite events, seismic activity in the area cannot be considered as the
545 exclusive potential triggering mechanism for the deposition of this high number of
546 homogenites.

547 Comparison of homogenites with sediments accumulated at the deepest sub-basins (B1
548 and B2), corresponding to cores BAN-12-1 and 2, reflects many textural and compositional
549 similarities from the macroscopic scale, as observed in core images (Figs. 3, 4, 6B) to the
550 microscopic level, as observed in SEM images. These homogenites are also similar to the
551 "homogeneous sections" described by Leroy (2008) in the early Pleistocene sections of
552 Banyoles paleolake, likely deposited by a similar mechanism. Although the range of variation
553 in grain size is relatively small in general, and within unit C in particular, homogenites are
554 slightly coarser (Fig. 3), with values closer to BAN-12-1 and 2, averaging 8.6 and 9.6 μm,
555 respectively. From the compositional point of view, Ti/Ca ratios of lithotype 4 and short cores
556 BAN-12-1 and 2 are also similar and generally lower than lithotype 1 (Fig. 6B). Thus, a
557 common sediment source between B1 and B2 and homogenites is suggested. The marginal
558 location of core BAN-11-1A within the flat platform between B1 and B2 might explain this
559 decreasing grain size from B1 and B2 (8.6 μm and 9.6 μm), as coarsest particles transported
560 by turbidity plumes do not probably reach this area, as predicted by previous studies (Serra et
561 al., 2002, 2005).

562 According to recent limnological monitoring, there is a permanent contribution of
563 sediment particles derived from turbidity plume developed above B1 (Colomer et al., 2001;
564 Serra et al., 2005). Particle sediment fluxes in areas near coring site BAN-11-1A, close to the
565 shallow platform margins, between B1 and B2, do not reach 5 g m^{-2} day^{-1} (Serra et al., 2002,
566 2005). Therefore, this plume might contribute to < 1 mm/year of sediment thickness in this
567 area and thus, is responsible for a relatively low importance contribution of particles,
568 decreasing in size and number towards lake platform marginal areas, where coring site BAN-
569 11-1A is located (Fig. 8). Consequently, the relatively low sedimentation rate produced by
570 this plume is not able to accumulate the high thickness of homogenite sediments. In fact,
571 reddish, massive grained silts derived from B1 are spatially restricted to the edges of this sub-

572 basin and they do not normally reach more than 50 m from the source area (Fig. 8).
573 Furthermore, the frequent but episodic deposition of these homogenites must result from an
574 episodic and relatively rapid process rather than from a continuous, variable permanent
575 depositional mechanism.

576 In contrast, the second and stronger plume developed periodically above B2, as a result of
577 extraordinary intense groundwater inflow caused by intense rainfall in the recharge area of the
578 aquifer (Soler et al., 2009), has a particle sediment flux of 156 g m^2 day^{-1} (one order of
579 magnitude higher than B1), so that it is able to accumulate more than 1 cm of sediments per
580 year in the marginal areas of the platform located between B1 and B2. Taking into account
581 that homogenite thicknesses display a high range of variability (from 2 to 76 cm) and the
582 expected variability in the flow velocity for this turbidity plume, associated with the variable
583 diameter of karstic conducts within B2, this is the most likely depositional mechanism able to
584 produce homogenites.

585 In fact, correlation between short cores recovered between B1 and B2 and seismic line
586 (Fig. 8) document how most of the uppermost homogenites (reflected as transparent seismic
587 facies) are ponding predominantly towards sub-basin B2 and get thinner towards the edge of
588 the lake and B1. This depositional pattern suggests fluidization and resuspension of sediments
589 in sub-basin B2 as a result of particularly intense rainfall episodes in the recharge area of the
590 aquifer as the most likely mechanism for the deposition of homogenites in Lake Banyoles.

591

592 *5.2 Chronology and paleoenvironmental significance of homogenites*

593 According to ^{137}Cs and ^{210}Pb dating, no discrete layers associated with the 11 fluidization
594 events monitored in B2 during the period 1976-2004 AD (Soler et al., 2007) have been
595 recorded in core BAN-11-1A (Fig. 7). However, a detailed inspection of core images reveals
596 an internal irregular ‘sublayering’ of mm to sub-mm thick laterally discontinuous light grey

597 silts within black, massive, carbonate-rich silts of lithotype 1 (Figs. 4A, 8B). These small
598 amounts of light grey silt sediments might be derived from sub-basin B2 and have reached
599 coring site. Therefore, more intense groundwater inflow (or smaller karstic subaquatic springs
600 within sub-basin B2) is required to produce a denser turbidity plume than the ones monitored
601 during the last years (Soler et al., 2007) so that these 17 layers within uppermost unit LC
602 could be deposited. Alternatively, a longer duration for these events could produce thick
603 homogenite layers. However, we would expect some internal structure in the sediment layers
604 if the events lasted several years, and the lack of clear internal structure within these layers
605 make such a long lasting, permanent turbidity plume rather unlikely.

606 The different age models proposed for the uppermost unit containing the homogenites
607 (Fig. 7B), indicate that they were deposited between the 4^{th} and 20^{th} centuries AD.
608 Chronological uncertainties associated with the lack of reliable radiocarbon dates within this
609 interval hamper an accurate dating of these depositional events. In model 1, ^{137}Cs and ^{210}Pb
610 inferred sedimentation rate is unlikely to remain constant throughout several millennia
611 characterized by changing land use and climate. According to model 2, the linear interpolation
612 with the validated date of ~2800 cal yrs BP implies an unlikely abrupt change prior to 1963
613 AD and also a constant sedimentation rate through the intervals containing different
614 lithologies: i) alternating lithotypes 1 and 4 (upper part of the succession) and ii) banded to
615 laminated lithotype 2 (lower part of the succession). Finally, the exclusive validation of the
616 lowermost radiocarbon date within unit LC is arbitrary as all the others were rejected for the
617 potential recycling of material derived from resuspension (Table 2, Fig. 7).

618 A fluctuating, long-term increase in lake level in Banyoles is evidenced by the onlapping
619 of unit LC over units LA and LB, containing shallower deposits (Figs. 2, 3). This is also
620 supported by the existence of a submerged early Neolithic settlement in the eastern shore of
621 the lake (La Draga site). This archeological site is constituted by lakeshore type houses dated

622 as old as ~7200 cal. BP by radiocarbon (Bosch et al., 2000; Tarrús, 2008), and implies that
623 lake level was up to 1.5 m lower than the current level during the Early Neolithic.

624 A drastic change in depositional environments occurred at the base of Unit C, at ~2.8 cal
625 ka BP, and inaugurated a new lake dynamics favorable to homogenite formation. Although
626 the timing is coherent with a large increase in humidity - particularly in southern Spain
627 (Martín-Puertas et al., 2009) –documented at the onset of the Iberian-Roman Humid Period
628 (ca. 2.5 cal ka BP), moisture conditions have been quite variable during the last two millennia
629 in the Iberian Peninsula in general (Moreno et al., 2012) and NE Spain in particular (Morellón
630 et al., 2012). Thus, a direct, exclusive climate driven hydrological change for the deposition of
631 homogenites can be ruled out. However we cannot discard the possibility that changes in the
632 karst functioning with new preferential areas for spring flow brought by the onset of this
633 humid period could have become permanent and favored homogenite formation during the
634 last three millennia.

635 The presence of several homogenites at the lowermost part of the recovered sequence,
636 between ~5450 and 7200 cal yrs BP suggest that, apart from the autogenic evolution of these
637 karstic depressions described by Canals et al. (1990), an external hydrological mechanism
638 would be required for such a depositional change. In fact, no homogenites have been
639 identified near to the other sub-basins of the lake by geophysical surveys and sediment cores.
640 Thus, a higher, local groundwater discharge likely caused by a faster recharge of the aquifer
641 might have activated sub-basin B2, causing these episodic, more intense fluidization events
642 and associated turbidity plumes in Lake Banyoles during the last millennium. Without a more
643 detailed age model, the onset of homogenite deposition could have started as early as the
644 humid Iberian-Roman Period or as late as Medieval times. In the second case, it would have
645 been coincident with the human settlement of the area and associated changes in land use and
646 lake hydrology. The foundation of Sant Esteve Monastery in the town of Banyoles (Sanz i

Alguacil, 1991) in the early 9th century AD led to large changes in the lake and the watershed, as the construction of an artificial drainage system (five artificial outlets and several dikes in the eastern shore of the lake) to control lake level. Moreover, intense deforestation and farming affected the catchment drainage and permeability. A local expansion of agriculture occurred in relation to the foundation of another Romanesque monastery in the town of Besalu (960 AD), located in the recharge area of the aquifer (Sanz, 1981).

Deforestation caused by the important expansion of farmlands in the region and associated increase in soil permeability in the recharge area of the aquifer might have led to a faster recharge of the karstic system feeding Lake Banyoles, increasing its rapid hydrological response to intense rainfall episodes responsible for fluidization episodes in sub-basin B2 and favoring the deposition of homogenites. Higher groundwater inflow through the spring located in sub-basin B2 could be responsible for more intense fluidization events and associated turbidity plumes. Progressive farmland abandonment and associated reforestation during the mid to late 20th century and/or groundwater extraction might have lowered water table, decreasing the intensity of fluidization events in B2 sub-basin during recent times and thus, preventing the deposition of homogenites.

6. Conclusions

Recent sedimentary processes in karstic Lake Banyoles are strongly influenced by the effect of groundwater activity, which leads to fluidization, re-suspension and mainly vertical transport and gravity of sediment particles forming homogenite deposits accumulated in the platforms between deepest sub-basins B1 and B2. These processes are permanent in B1 and periodic in B2, respectively. Based on high-resolution geophysical surveys and detailed sedimentological and geochemical analyses of several cores, we document a large variability

671 in the intensity and frequency of these transport processes and the subsequent deposition of
672 homogenite layers during the last millennium.

673 The ~7.6 cal kyr BP recovered sequence of Lake Banyoles has recorded an increase in
674 lake level after ~2800 cal yrs BP, as indicated by geophysical (i.e., the onlapping of
675 uppermost unit SC onto lowermost units SA and SB) and sedimentological (i.e., change from
676 massive, carbonate-rich shallow lake deposits into fine-grained, clastic-rich sediments)
677 evidences. This lake level change was accompanied by a subsequent intensification of
678 groundwater input and the deposition of 17 layers of homogenites that are up to 75 cm thick.

679 Textural and compositional analysis and depositional patterns of homogenites indicate
680 that they have been deposited by periodical, intense, fluidization events in sub-basin B2 as
681 those described and monitored for recent times. Intensity, however, was higher, able to
682 generate thicker, discrete layers in marginal areas of the platform between the deepest sub-
683 basins in the southern basin of the lake. The onset of these events was triggered by higher and
684 more intense local, groundwater inflow and might be related to agricultural expansion during
685 Roman and/or medieval times in the region. Increased farmland surface in the recharge area
686 of the aquifer increased soil permeability and subsequently, the rapid response of the aquifer
687 to intense rainfall episodes in the recharge area.

688

689 **Acknowledgements**

690 Financial support for research was provided by the Spanish Inter-Ministry
691 Commission of Science and Technology (CICYT), through the projects GLOBALKARST
692 (CGL2009-08415) and GRACCIE-CONSOLIDER (CSD2007-00067). Additional funding
693 was provided by INTIMATE-COST through a travel grant ‘Short Term Scientific Mission,
694 COST Action ES0907’ in 2011 at IPE-CSIC and University of Barcelona (Spain).

M. Morellón and F. Barreiro hold ‘JAE-DOC’ and ‘JAE-PREDOC’ pre and postdoctoral contracts, respectively, both co-funded by C.S.I.C. and the European Social Fund. We acknowledge the Town Hall of Banyoles (Girona) and Club Natació Banyoles for their collaboration in fieldwork activities and Jaime Frigola and Pol Tarrats (Univ. of Barcelona), and Miguel Sevilla and Josu Aranbarri (IPE-CSIC) for coring assistance in 2011. We are also grateful to Irene Brunner, Silvia Bollhalder, Marian Fujak, Alois Zwyssig and Brian Sinnet (Eawag, Switzerland); Adrian Gilli and Stephanie Wirth (ETH-Zürich, Switzerland) and Beatriz Bueno, Aida Adsuar and Miguel Bartolomé (IPE-CSIC, Spain) for their laboratory assistance and collaboration in this research. We thank constructive comments on the manuscript made by Maria Rieradevall (Univ. of Barcelona). We also acknowledge anonymous reviewers for their helpful comments and their criticism, which led to a considerable improvement in the manuscript.

REFERENCES

Álvarez-Cobelas, M., Rojo, C., Angeler, D.G., 2005. Mediterranean limnology: current status, gaps and the future. Journal of Limnology 64, 13-29.

Assayag, N., Jézéquel, D., Ader, M., Viollier, E., Michard, G., Prévot, F., Agrinier, P., 2008. Hydrological budget, carbon sources and biogeochemical processes in Lac Pavin (France): Constraints from $\delta^{18}O$ of water and $\delta^{13}C$ of dissolved inorganic carbon. Applied Geochemistry 23, 2800-2816.

Barnolas, A., 1992. Evolución sedimentaria de la Cuenca Surpirenaica Oriental durante el Eoceno. Acta Geologica Hispanica 27, 15-31.

Beck, C., 2009. Late Quaternary lacustrine paleo-seismic archives in north-western Alps: Examples of earthquake-origin assessment of sedimentary disturbances. Earth-Science Reviews 96, 327-344.

721 Bischoff, J.L., Julià, R., Shanks, W.C., Rosenbauer, R.J., 1994. Karstification without
722 carbonic acid: Bedrock dissolution by gypsum-driven dedolomitization. Geology 22,
723 995-998.
724 Bloesch, J., 1995. Mechanisms, measurement and importance of sediment resuspension in
725 lakes. Marine and Freshwater Research 46, 295-304.
726 Bosch, A., Chinchilla, J., Tarrús, J., 2000. El Poblat Lacustre Neolitic de la Draga:
727 Excavaciones de 1990 a 1998. Museu d'Arqueologia de Catalunya-Centre
728 d'Arqueologia Subaquàtica de Catalunya, Girona, Girona (Spain).
729 Brusi, D., Bach, J., Sanz, M., 1990. Itinerari geològic de Banyoles. Descoberta del
730 funcionament del sistema lacustre. Apunts 22. Eumo Editorial, Barcelona, 124 pp.
731 Burbank, D.W., Puigdefàbregas, C., Muñoz, J.A., 1992. The chronology of the Eocene
732 tectonic and stratigraphic development of the eastern Pyrenean foreland basin,
733 northeast Spain. Geological Society of America Bulletin 104, 1101-1120.
734 Burne, R.V., Moore, L.S., 1987. Microbialites; organosedimentary deposits of benthic
735 microbial communities. PALAIOS 2, 241-254.
736 Canals, M., Got, H., Julia, R., Serra, J., 1990. Solution-collapse depressions and suspensates
737 in the limnocrenic lake of Banyoles (NE Spain). Earth Surface Processes and
738 Landforms 15, 243-254.
739 Casamitjana, X., Colomer, J., Roget, E., Serra, T., 2006. Physical Limnology in Lake
740 Banyoles. Limnetica 25, 181-188.
741 Casamitjana, X., Colomer, J., Roget, E., Teresa, S., 1996. On the presence of aggregates in
742 the basins of Lake Banyoles. Geophysical Research Letters 23, 2737-2740.
743 Casamitjana, X., Roget, E., 1993. Resuspension of sediment by focused groundwater in Lake
744 Banyoles. Limnology and Oceanography 38, 643-656.

745 Colomer, J., Ross, J.A., Casamitjana, X., 1998. Sediment entrainment in karst basins. Aquatic
746 Sciences 60, 338-358.
747 Colomer, J., Serra, T., Piera, J., Roget, E., Casamitjana, X., 2001. Observations of a
748 hydrothermal plume in a karstic lake. Limnology and Oceanography 46, 197-203.
749 Colomer, J., Serra, T., Soler, M., Casamitjana, X., 2002. Sediment fluidization events in a
750 lake caused by large monthly rainfalls. Geophysical Research Letters 29, 101/1-101/3.
751 Coma, M.V., Abella, C.A., Oromi, O., 1988. Caracteritzacio fisico-quimica dels travertins en
752 formació de l'Estany de Banyoles. Scientia Gerundensis 14, 43-56.
753 Coma, M.V., Oromi, O., Abella, C.A., 1987. Cartografia dels travertins en formació de
754 l'Estany de Banyoles. Scientia Gerundensis 13, 65-74.
755 Cho Martínez, S., 2012. Registros sedimentarios como indicadores paleoambientales y de
756 actividad antrópica en el Neolítico del Lago de Banyoles. Master Thesis, Universidad
757 de Burgos Burgos (Spain), 48 pp.
758 Chung, F.H., 1974a. Quantitative interpretation of X-ray diffraction patterns of mixtures. I.
759 Matrix-flushing method for quantitative multicomponent analysis. Journal of Applied
760 Crystallography 7, 519-525.
761 Chung, F.H., 1974b. Quantitative interpretation of X-ray diffraction patterns of mixtures. II.
762 Adiabatic principle of X-ray diffraction analysis of mixtures. Journal of Applied
763 Crystallography 7, 526-531.
764 Dadheech, P.K., Glöckner, G., Casper, P., Kotut, K., Mazzoni, C.J., Mbedi, S., Krienitz, L.,
765 2013. Cyanobacterial diversity in the hot spring, pelagic and benthic habitats of a
766 tropical soda lake. FEMS Microbiology Ecology 85, 389-401.
767 Descy, J.-P., Darchambeau, F., Schmid, M., 2012a. Lake Kivu Research: Conclusions and
768 Perspectives. In: Descy, J.-P., Darchambeau, F., Schmid, M. (Eds.), Lake Kivu.
769 Aquatic Ecology Series 5, Springer, Dordrecht, (Netherlands), pp. 181-190.

770 Descy, J.-P., Darchambeau, F., Schmid, M. (Eds.), 2012b. Lake Kivu. Limnology and
771 biogeochemistry of a tropical great lake. Aquatic Ecology Series 5. Springer,
772 Dordrecht, (Netherlands).
773 Draganits, E., Janda, C., 2003. Subaqueous artesian springs and associated spring pits in a
774 Himalayan pond. Boreas 32, 436-442.
775 Dutras, A., Abella, C., Brunet, R., 1986. Determinació del sistema de corrents a l'Estany de
776 Banyoles en condiciones de calma meteorològica estival. Primeres jornades sobre
777 l'Estany de Banyoles. Ponències i comunicacions, Banyoles (Spain), pp. 149-157.
778 Edmunds, W.M., Dodo, A., Djoret, D., Gaye, C., Goni, I., Travi, Y., Zouari, K., Zuppi, G.-
779 M., Gasse, F., 2004. Groundwater as an archive of climatic and environmental change:
780 Europe to Africa. In: Battarbee, R., Gasse, F., Stickley, C. (Eds.), Past Climate
781 Variability through Europe and Africa. Developments in Paleoenvironmental Research
782 6, Springer, Dordrecht, (Netherlands) pp. 279-306.
783 Garcia-Gil, L.J., Borrego, C.M., Bañeras, L., Abella, C.A., 1993. Dynamics of Phototrophic
784 Microbial Populations in the Chemocline of a Meromictic Basin of Lake Banyoles.
785 Internationale Revue der gesamten Hydrobiologie und Hydrographie 78, 283-294.
786 García-Ruiz, J.M., López-Moreno, J.I., Vicente-Serrano, S.M., Lasanta-Martínez, T.,
787 Beguería, S., 2011. Mediterranean water resources in a global change scenario. Earth-
788 Science Reviews 105, 121-139.
789 Girardclos, S., Schmidt, O.T., Sturm, M., Ariztegui, D., Pugin, A., Anselmetti, F.S., 2007.
790 The 1996 AD delta collapse and large turbidite in Lake Brienz. Marine Geology 241,
791 137-154.
792 Guerrero, R., Abella, C., Miracle, M.R., 1978. Spatial and temporal distribution of bacteria in
793 a meromictic karstic lake basin: relationships with physicochemical parameters and
794 zooplankton. Verhandlungen des Internationalen Verein Limnologie 20, 2264-2271.

795 Höbig, N., Weber, M.E., Kehl, M., Weniger, G.-C., Julià, R., Melles, M., Fülöp, R.-H.,
796 Vogel, H., Reicherter, K., 2012. Lake Banyoles (northeastern Spain): A Last Glacial to
797 Holocene multi-proxy study with regard to environmental variability and human
798 occupation. Quaternary International 274, 205-218.
799 Hsü, K.J., Kelts, K., 1985. Swiss lakes as a geological laboratory. Naturwissenschaften 72(6),
800 315-321.
801 Ionescu, D., Siebert, C., Polerecky, L., Munwes, Y.Y., Lott, C., Häusler, S., Bižić-Ionescu,
802 M., Quast, C., Peplies, J., Glöckner, F.O., Ramette, A., Rödiger, T., Dittmar, T., Oren,
803 A., Geyer, S., Stärk, H.-J., Sauter, M., Licha, T., Laronne, J.B., de Beer, D., 2012.
804 Microbial and Chemical Characterization of Underwater Fresh Water Springs in the
805 Dead Sea. PLoS ONE 7(6), e38319.
806 Julià-Brugués, R., 1977. Nuevos datos sobre la posicion cronoestratigráfica de los materiales
807 cuaternarios de la cuenca lacustre de Banyoles-Besalú (Girona). Acta Geológica
808 Hispánica XII, 55-59.
809 Julia Bruguès, R., Suc, J.-P., 1980. Analyse pollinique des dépôts lacustresdu Pléistocène
810 inférieur de Banyoles (Bañolas, site de la Bòbila Ordis - Espagne): un élément
811 nouveau dans la reconstitution de l'histoire paléoclimatique des régions
812 méditerranéennes d'Europe occidentale. Geobios 13, 5-19.
813 Julià, R., 1980. La conca lacustre de Banyoles Centro d'Estudios Comarcals de Banyoles,
814 Besalu, 188 pp.
815 Julià, R., Bischoff, J.L., 1991. Radiometric dating of quaternary deposits and the hominid
816 mandible of lake banyolas, Spain. Journal of Archaeological Science 18, 707-722.
817 Leroy, S., 1990. Paléoclimats plio-pléistocènes en Catalogne et Languedoc d'après la
818 palynologie de formations lacustres. Thèse de doctorat en science Thesis, UCL, 512
819 pp.

820 Leroy, S.A.G., 1997. Climatic and non-climatic lake-level changes inferred from a Plio-
821 Pleistocene lacustrine complex of Catalonia (Spain): palynology of the Tres Pins
822 sequences. Journal of Paleolimnology 17, 347-367.
823 Leroy, S.G., 2008. Vegetation cycles in a disturbed sequence around the Cobb-Mountain
824 subchron in Catalonia (Spain). Journal of Paleolimnology 40, 851-868.
825 Løvlie, R., Leroy, S., 1995. Magnetostratigraphy of Lower Pleistocene Banyoles palaeolake
826 carbonate sediments from Catalonia, NE Spain: Evidence for relocation of the Cobb
827 Mountain sub-chron. Quaternary Science Reviews 14, 473-485.
828 MAGRAMA, 2006. Information Sheet on Ramsar Wetlands: Lake Banyoles, 21 pp.
829 Martín-Puertas, C., Valero-Garcés, B.L., Brauer, A., Mata, M.P., Delgado-Huertas, A.,
830 Dulski, P., 2009. The Iberian-Roman Humid Period (2600-1600 cal yr BP) in the
831 Zoñar Lake varve record (Andalucía, southern Spain). Quaternary Research 71, 108-
832 120.
833 Mató i Palós, E., Saula i Briansó, E., Picart i Boira, J., Solà i Subiranas, J., Montaner i
834 Roviras, J., Viñals i Gisbert, E., Samsó i Escolá, J.M., Serra i Kiel, J., Llenas i
835 Abellaneda, M., Agustí i Ballester, J., Mallarach i Carrera, J., 1996. Banyoles 295-2-1
836 (76,23). In: Berástegui Batalla, X., Losantos Sistach, M., Cirés, J. (Eds.), Mapa
837 geològic de Catalunya 1:25000. Generalitat de Catalunya, Departament de Politica
838 Territorial i Obres Públiques, Institut Cartográfic de Catalunya, Servei Geològic de
839 Catalunya, Barcelona (Spain).
840 Matter, M., Anselmetti, F.S., Jordanoska, B., Wagner, B., Wessels, M., Wüest, A., 2010.
841 Carbonate sedimentation and effects of eutrophication observed at the Kališta
842 subaquatic springs in Lake Ohrid (Macedonia). Biogeosciences 7, 3755-3767.
843 Morellón, M., Pérez-Sanz, A., Corella, J.P., Büntgen, U., Catalán, J., González-Sampériz, P.,
844 González-Trueba, J.J., López-Sáez, J.A., Moreno, A., Pla-Rabes, S., Saz-Sánchez,

845 M.Á., Scussolini, P., Serrano, E., Steinhilber, F., Stefanova, V., Vegas-Vilarrúbia, T.,
846 Valero-Garcés, B., 2012. A multi-proxy perspective on millennium-long climate
847 variability in the Southern Pyrenees. Climate of the Past 8, 683-700.
848 Morellón, M., Valero-Garcés, B., Anselmetti, F., Ariztegui, D., Schnellmann, M., Moreno, A.,
849 Mata, P., Rico, M., Corella, J.P., 2009. Late Quaternary deposition and facies model
850 for karstic Lake Estanya (North-eastern Spain). Sedimentology 56, 1505-1534.
851 Moreno-Amich, R., García-Berthou, E., 1989. A new bathymetric map based on echo-
852 sounding and morphometrical characterization of the Lake of Banyoles (NE-Spain).
853 Hydrobiologia 185, 83-90.
854 Moreno, A., Pérez, A., Frigola, J., Nieto-Moreno, V., Rodrigo-Gámiz, M., Martrat, B.,
855 González-Sampériz, P., Morellón, M., Martín-Puertas, C., Corella, J.P., Belmonte, Á.,
856 Sancho, C., Cacho, I., Herrera, G., Canals, M., Grimalt, J.O., Jiménez-Espejo, F.,
857 Martínez-Ruiz, F., Vegas-Vilarrúbia, T., Valero-Garcés, B.L., 2012. The Medieval
858 Climate Anomaly in the Iberian Peninsula reconstructed from marine and lake records.
859 Quaternary Science Reviews 43, 16-32.
860 Olivera, C., Redondo, E., Lambert, J., Riera, A., Roca, A., 2006. Els terratrèmols dels segles
861 XIV i XV a Catalunya. Institut Cartogràfic de Catalunya, Barcelona.
862 Paillard, D., Labeyrie, L., Yiou, P., 1996. Analyseries 1.0: a Macintosh software for the
863 analysis of geographical time-series. Eos 77, 379.
864 Pérez-Obiol, R., Julià, R., 1994. Climatic Change on the Iberian Peninsula Recorded in a
865 30,000-Yr Pollen Record from Lake Banyoles. Quaternary Research 41, 91-98.
866 Prat, N., Rieradevall, M., 1995. Life cycle and production of Chironomidae (Diptera) from
867 Lake Banyoles (NE Spain). Freshwater Biology 33, 511-524.
868 Reimer, P.J., Baillie, M.G.L., Bard, E., Bayliss, A., Beck, J.W., Blackwell, P.G., Ramsey,
869 C.B., Buck, C.E., Burr, G.S., Edwards, R.L., Friedrich, M., Grootes, P.M., Guilderson,

870 T.P., Hajdas, I., Heaton, T.J., Hogg, A.G., Hughen, K.A., Kaiser, K.F., Kromer, B.,
871 McCormac, F.G., Manning, S.W., Reimer, R.W., Richards, D.A., Southon, J.R.,
872 Talamo, S., Turney, C.S.M., van der Plicht, J., Weyhenmeyer, C.E., 2009. IntCal09
873 and Marine09 Radiocarbon Age Calibration Curves, 0-50,000 Years cal BP.
874 Radiocarbon 51, 1111–1150.
875 Rieradevall, M., Roca, J.R., 1995. Distribution and population dynamics of ostracodes in a
876 Karstic lake: Lake Banyoles (Catalonia, Spain). Hidrobiología 310, 189-196.
877 Roget, E., Colomer, J., Casamitjana, X., Llebot, J.E., 1993. Bottom currents induced by
878 baroclinic forcing in Lake Banyoles (Spain). Aquatic Sciences - Research Across
879 Boundaries 55, 206-227.
880 Rosen, M.R., Arehart, G.B., Lico, M.S., 2004. Exceptionally fast growth rate of <100-yr-old
881 tufa, Big Soda Lake, Nevada: Implications for using tufa as a paleoclimate proxy.
882 Geology 32, 409-412.
883 Rosen, M.R., Chagué-Goff, C., Eser, P., Coshell, L., 2002. Utilisation of the sedimentological
884 and hydrochemical dynamics of the Stump Bay Wetland along Lake Taupo, New
885 Zealand, for the recognition of paleo-shoreline indicators. Sedimentary Geology 148,
886 357-371.
887 Ross, K.A., Smets, B., De Batist, M., Hilbe, M., Schmid, M., Anselmetti, F.S., 2014. Lake-
888 level rise in the late Pleistocene and active subaquatic volcanism since the Holocene in
889 Lake Kivu; East African Rift. Geomorphology, in press. DOI:
890 10.1016/j.geomorph.2014.05.010
891 Sanz i Alguacil, A., 1991. Catalunya Romanica. Vol V. El Gironès, la Selva, el Pla de
892 l'Estany, Enciclopèdia Catalana.
893 Sanz, M., 1981. El sistema hidrogeológico de Banyoles-La Garrotxa. Unpublished PhD thesis,
894 Universitat Autònoma de Barcelona, Barcelona, Spain.

895 Saula, E., Picart, J., Mato, E., Llenas, M., Lozanitos, M., Beràstegui, X., Agustí, J., 1994.
896 Evolución geodinámica de la fosa del Empordà y las Sierras Transversales. Acta
897 Geologica Hispanica 29, 55-75.
898 Schnellmann, M., Anselmetti, F.S., Giardini, D., McKenzie, J.A., 2005. Mass movement-
899 induced fold-and-thrust belt structures in unconsolidated sediments in Lake Lucerne
900 (Switzerland). Sedimentology 52, 271-289.
901 Schnurrenberger, D., Russell, J., Kelts, K., 2003. Classification of lacustrine sediments based
902 on sedimentary components. Journal of Paleolimnology 29, 141-154.
903 Secanell, R., Goula, X., Susagna, T., Fleta, J., Roca, A., 2004. Seismic hazard zonation of
904 Catalonia, Spain, integrating random uncertainties. Journal of Seismology 8(1), 25-40.
905 Serra-Kiel, J., Travé, A., Mató, E., Saula, E., Ferràndez-Cañadell, C., Busquets, P., Tosquella,
906 J., Vergés, J., 2003. Marine and Transitional Middle/Upper Eocene Units of the
907 Southeastern Pyrenean Foreland Basin (NE Spain). Geologica Acta 1(2), 177-200.
908 Serra, T., Colomer, J., Gacia, E., Soler, M., Casamitjana, X., 2002. Effects of a turbid
909 hydrothermal plume on the sedimentation rates in a karstic lake. Geophysical
910 Research Letters 29, 2029.
911 Serra, T., Soler, M., Julià, R., Casamitjana, X., Colomer, J., 2005. Behaviour and dynamics of
912 a hydrothermal plume in Lake Banyoles, Catalonia, NE Spain. Sedimentology 52,
913 795-808.
914 Shapley, M.D., Ito, E., Donovan, J.J., 2005. Authigenic calcium carbonate flux in
915 groundwater-controlled lakes: Implications for lacustrine paleoclimate records.
916 Geochimica et Cosmochimica Acta 69, 2517-2533.
917 Soler, M., Serra, T., Casamitjana, X., Colomer, J., 2009. High sedimentation rates in a karstic
918 lake associated with hydrothermal turbid plumes (Lake Banyoles, Catalonia, NE
919 Spain). Sedimentary Geology 222, 5-15.

920 Soler, M., Serra, T., Colomer, J., Romero, R., 2007. Anomalous rainfall and associated
921 atmospheric circulation in the northeast Spanish Mediterranean area and its
922 relationship to sediment fluidization events in a lake. Water Resources Research 43,
923 W01404.
924 Tarrús, J., 2008. La Draga (Banyoles, Catalonia), an Early Neolithic Lakeside Village in
925 Mediterranean Europe. Catalan Historical Review 1, 17-33.
926 Tassone, A., Roca, E., Muñoz, J.A., Cabrera, L., Canals, M., 1994. Evolución del sector
927 septentrional del margen continental catalán durante el Cenozoico Acta Geologica
928 Hispanica 29, 3-7.
929 Valero-Garcés, B., Morellón, M., Moreno, A., Corella, P., Martín-Puertas, C., Barreiro, F.,
930 Pérez, A., Giralt, S., Mata-Campo, M.P., 2014. The carbonate factory in karst lakes:
931 sources, processes and depositional environments in Quaternary Iberian Lakes.
932 Sedimentary Geology 299, 1-29.
933 Valero-Garcés, B., Zeroual, E., Kelts, K., 1998. Arid phases in the Western Mediterranean
934 Region during the last glacial cycle reconstructed from lacustrine records. In: Benito,
935 G., Baker, V.R., Gregory, K.J. (Ed.), Palaeohydrology and Environmental Change,
936 John Wiley & Sons Ltd., pp. 67-80.
937 Warren, J.K., 1982. The hydrological significance of Holocene tepees, stromatolites, and
938 boxwork limestones in coastal salinas in South Australia. Journal of Sedimentary
939 Research 52, 1171-1201.
940 Winter, T.C., 1999. Relation of streams, lakes, and wetlands to groundwater flow systems.
941 Hydrogeology Journal 7, 28-45.
942 Younger, P.L., Teutsch, G., Custodio, E., Elliot, T., Manzano, M., Sauter, M., 2002a.
943 Assessments of the sensitivity to climate change of flow and natural water quality in
944 four major carbonate aquifers of Europe. In: Hiscock, K.M., Rivett, M.O., Davison,

945 R.M. (Eds.), Sustainable Groundwater Development. Geological Society, London,
946 Special Publications 193, pp. 303-323.
947 Younger, P.L., Teutsch, G., Custodio, E., Elliot, T., Manzano, M., Sauter, M., 2002b.
948 Assessments of the sensitivity to climate change of flow and natural water quality in
949 four major carbonate aquifers of Europe. Geological Society, London, Special
950 Publications 193, 303-323.
951

TABLE CAPTIONS

	Lithotype	*Sedimentological features*	*Composition parameters*	*Depositional subenvironment/ process*
Banded and laminated	**1**	***Dark-grey to black, massive to banded, carbonate-rich silts with diatoms*** Fine grained carbonate mud composed by up to 10 µm hexagonal calcite grains with abundant to frequent ca. 50-60 µm reworked occasional reworked littoral carbonate-rich particles (ostracods, charophytes and carbonate coatings). Frequent ca. 25 µm detrital carbonate particles, plant remains and diatoms, locally abundant. Occasional quartz grains and < 20µm pyrite framboids.	**TIC** = 3.3% - 6.7 % **TOC** = 0.0% - 1.2 % **Mean GS** = 5 – 18 µm **Mineralogy**: **Cc**= 42.3%, **Ill** = 32.5%, **Chl**= 17.7%, **Qtz**= 7.4%	Deep, monomictic, occasionally anoxic brackish to freshwater lake with permanent, low-concentration turbidity plumes
	2	***Laminated fcs comprising alternating mm to 1 cm thick black and light-grey fine-grained silts*** Black laminae: Fine-grained (up to 10 µm) hexagonal to sub-hexagonal calcite grains with abundant diatoms, up to 100 µm reworked littoral carbonate particles and frequent 20-30 µm detrital grains of quartz and carbonates. Light grey laminae: fine-grained, up to 10 µm irregular, reworked calcite crystals with frequent up to 40 µm clastic quartz and non-biogenic carbonates. Occasional to frequent up to 50 µm reworked littoral carbonate-rich particles.	**TIC =** 3.9 % – 6.2 % **TOC** = 0.2 %- 1.1 % **Mean GS =** 6.0 – 8.4 µm **Mineralogy: Cc** = 39.5%, **Ill** = 32.7%, **Chl** = 19.5%, **Qtz** = 8.2%	Relatively deep, carbonate-producing lake with seasonal anoxic hypolimnetic conditions
	3	***Grey, barely laminated to massive, carbonate-rich silts with evidences of bioturbation*** 30-50 µm reworked biogenic carbonate particles with abundant up to 50 µm irregularly shaped detrital grains of quartz and carbonates. Frequent fine-grained, up to 10 µm calcitic mud.	**TIC =** 4.4% – 9.3% **TOC** = 0.3%- 1.0 % **Mean GS** =4.8 – 18.9 µm **Mineralogy: Cc** = 51.6%, **Ill** = 26.5%, **Chl** = 15.1%, **Qtz** = 6.9%	Shallow, carbonate-producing brackish lake with oxic conditions
Massive	**4**	***Light grey, massive fine-grained, carbonate-rich silts, occurring as mm to cm-thick intercalations or cm to dm-thick homogeneous layers*** Up to 10 µm fine-grained irregularly-shaped calcite mud with abundant reworked diatoms. Frequent up to 50 µm reworked carbonate particles, sub-circular calcareous algae and pyrite framboids. Occasional plant remains.	**TIC =** 4.3% -6.8 % **TOC** = 0.1% - 0.9 % **Mean GS =** 5 – 12.6 µm **Mineralogy: Cc** = 44.7%, **Ill** = 31.7%, **Chl** = 16.2%, **Qtz** = 7.4%	Fluidization events and associated periodical and intense turbidity plumes

5	***Light grey/yellowish, massive, fine-grained, up to 1 m thick fining upwards sequences ranging from coarse to fine-grained silts*** Dominant 10-15 µm reworked, sub-rounded to hexagonal calcite grains with reworked littoral carbonate-rich particles (up to 50-60 µm), more frequent towards the base.	**TIC** = 4.5 % - 7.3% **TOC** = 0.3 % - 0.6 % **Mean GS** = 8.2 – 13.0 µm **Mineralogy: Cc** = 40.9%, **Ill** = 32.7%, **Chl** = 18.8%, **Qtz** = 7.7%	Mass-wasting processes
6	***Light grey/yellowish, massive, fine-grained, carbonate-rich sands*** 100-300 µm sub-rounded, biogenic, reworked carbonate particles with abundant up to 100 µm coarse, high relief detrital grains of quartz and non-biogenic carbonates. Abundant fine-grained matrix composed of up to 10 µm sub-rounded calcite crystals.	**TIC** = 7.2% - 8.8% **TOC** = 0.4% - 0.5 % **Mean GS** = 65.5 µm **Mineralogy: Cc** = 57.9%, **Chl** = 18.1%, **Ill** = 15.4%, **Qtz** = 8.6%	Mass-wasting processes

Table 1. Lithotypes defined for the Lake Banyoles sequence, including sedimentological features, main compositional parameters (TIC = Total Inorganic Carbon, TOC = Total Organic Carbon, GS = Grain Size and mineralogical content (%), including: quartz (Qtz), chlorite (Chl), illite (Ill) and calcite (Cc)) and depositional subenvironments and/or process interpreted for each case.

Comp depth (cm)	*Unit*	*Laboratory code*	*Type of material*	*AMS ^{14}C age (yr B.P.)*	*Corrected AMS ^{14}C age*	*Calibrated corrected age (cal yrs BP) (2σ range)*
44.5	LC	D-AMS 001611	Bulk organic matter	5460 ± 35	-13 ± 35	*Modern*
123	LC	D-AMS 001114	Bulk organic matter	6537 ± 36	1064 ± 71	984 ± 187
197.7	LC	D-AMS 001113	Bulk organic matter	5441 ± 33	-32 ± 68	*Modern*
290.5	LC	D-AMS 001609	Bulk organic matter	6519 ± 31	1046 ± 66	979 ± 187
528.8	LC	D-AMS 001112	Bulk organic matter	6217 ± 52	744 ± 87	723 ± 179
627.2	LB	D-AMS 001111	Bulk organic matter	5743 ± 39	2718 ± 324	2808 ± 802
996.1	LA	D-AMS 001610	Bulk organic matter	7813 ± 40	4788 ± 325	5453 ± 824
1297.9	LA	D-AMS 001110	Bulk organic matter	9790 ± 54	6765 ± 339	7600 ± 580
1297.9	LA	ETH-45854	Charcoal	6765 ± 285	6765 ± 285	7600 ± 580

Table 2. Radiocarbon dates used for the construction of the age model for the Lake Banyoles sequence. A correction of 3025 ± 35 ^{14}C years was applied to bulk sediment samples from units LA and LB, and 5473 ± 285 ^{14}C years to uppermost lithological unit LC. Corrected dates were calibrated using CALIB 6.0 software and the INTCAL09 curve (Reimer et al., 2009); and the mid-point of 95.4% (2σ probability interval) was selected.

FIGURE CAPTIONS

Fig. 1. (A) Location of the Lake Banyoles within the Iberian Peninsula; (B) bathymetric map, basins and sub-basins (modified from Soler et al., 2009); (C) aerial photograph with seismic grids obtained with the Pinger 3.5 khZ source (yellow) and Edgetech profiler (red), with indication of the seismic profile displayed below (dashed line), long (dots) and short core (squares) locations; and (D) S-N seismic profile.

Fig. 2. (A) W-E seismic section (line 4) and correlation with core BAN-11-1A indicated by superposition of core image, sedimentological profile (see legend below) and density profile (g/cm^3); (B) S-N seismic section (line 24) with core BAN-11-1A location and limits of seismic units marked by blue dotted lines; (C) Location of (A) and (B) in the seismic grid.

Fig. 3. Composite sequence for Lake Banyoles record (core BAN-11-1A). From left to right: core image, sedimentary units, sedimentological profile (see legend in Fig. 2 and lithotypes description in Table 1), lightness record (L*), magnetic susceptibility (MS) (SI units), total inorganic carbon (TIC), total organic carbon (TOC) (%), mineralogical composition (%), including: quartz (Qtz), chlorite (Chl), illite (Ill) and calcite (Cc) (see legend below); mean and mode grain size (μm), represented at absolute scale (lower part, bold line) and lower scale (upper part, thin, grey line) and grain size classes (sand, silt and clay) distribution (%) (see legend below). Homogenites and turbidite event layers are indicated by horizontal blue and orange bands, respectively.

Fig. 4: High resolution core images of the different lithotypes defined for the Lake Banyoles sequence: (A) lithotype 1; (B) lithotype 2; (C) lithotype 3; (D) lithotype 4; (E) alternation between lithotypes 1 and 4; (F) turbidite sequence composed by lithotypes 6 (base) and 5 (mid-top of the core section); (G) suspended sediments within sub-basin B1; and H, suspended sediments within sub-basin B2. Scale is in cm.

Fig. 5. Backscattered scanning electron images in selected intervals of cores BAN-11-1A, BAN-12-1 and 2. (A-C) Lithotype 1: (A) General view (3000x), (B) detail of endogenic carbonates (12000x), (C) detail of detrital grains and plant remains transported from the watershed (6000x). (D-F) Lithotype 4 (homogenites): (D) General view (3000x), (E) detail of a pyrite framboid (12000x), (F) detail of coccolithophorid remains transported from the calcareous bedrock of deepest sub-basin and reworked diatoms (12000x).

Fig. 6. (A) X-ray Fluorescence (XRF) scanner data of lithologic Unit LC. Element concentrations (Al, Si, Ti, Fe, Mn, Ca, Sr, S), expressed as counts per second, and Ti/Ca, Sr/Ca and Fe/Mn ratios are indicated. Core image, sedimentary units and sedimentological profile are also included (see legend in Fig. 2). Homogenites are indicated by horizontal blue bands. (B) Bipolar plot of Ca vs. Ti relationship along lithotypes 4 (homogenites), 1 and suspended sediments from short gravity cores BAN-11-1 and 2.

Fig. 7. (A) Chronological model of the composite sequence of Lake Banyoles, formed by long cores BAN-11-1A and short core 1A-1G, based on the linear interpolation of AMS ^{14}C dates (black and white dots) and 1963 AD maximum ^{137}Cs peak (star).

Material used for dating and rejected dates are also indicated in the legend. Different models proposed for the uppermost part (1, 2 and 3) correspond to red, green and blue lines, respectively. Homogenites and turbidite event layers are indicated by horizontal blue and orange bands, respectively. (B) ^{137}Cs and ^{210}Pb activity profiles for the uppermost 70 cm of the sequence. (C) Detail of age/depth relationships along the uppermost unit C.

Fig. 8. (A) Interpreted composite seismic profile between deepest sub-basins B1 and B2 with the location of short and long cores and interpreted deposits of homogenites derived from B1 (orange) and B2 (blue) sub-basins. (B) Correlation panel of short gravity cores (BAN-12-1, 2, 3, 4, 5, 6 and 8) and long core BAN-11-1A along a transect between sub-basins B1 and B2. Orange and blue-shaded areas represent correlation between homogenites derived from B1 and B2, respectively. (C) Core locations on the seismic grid in an aerial photograph of Lake Banyoles.

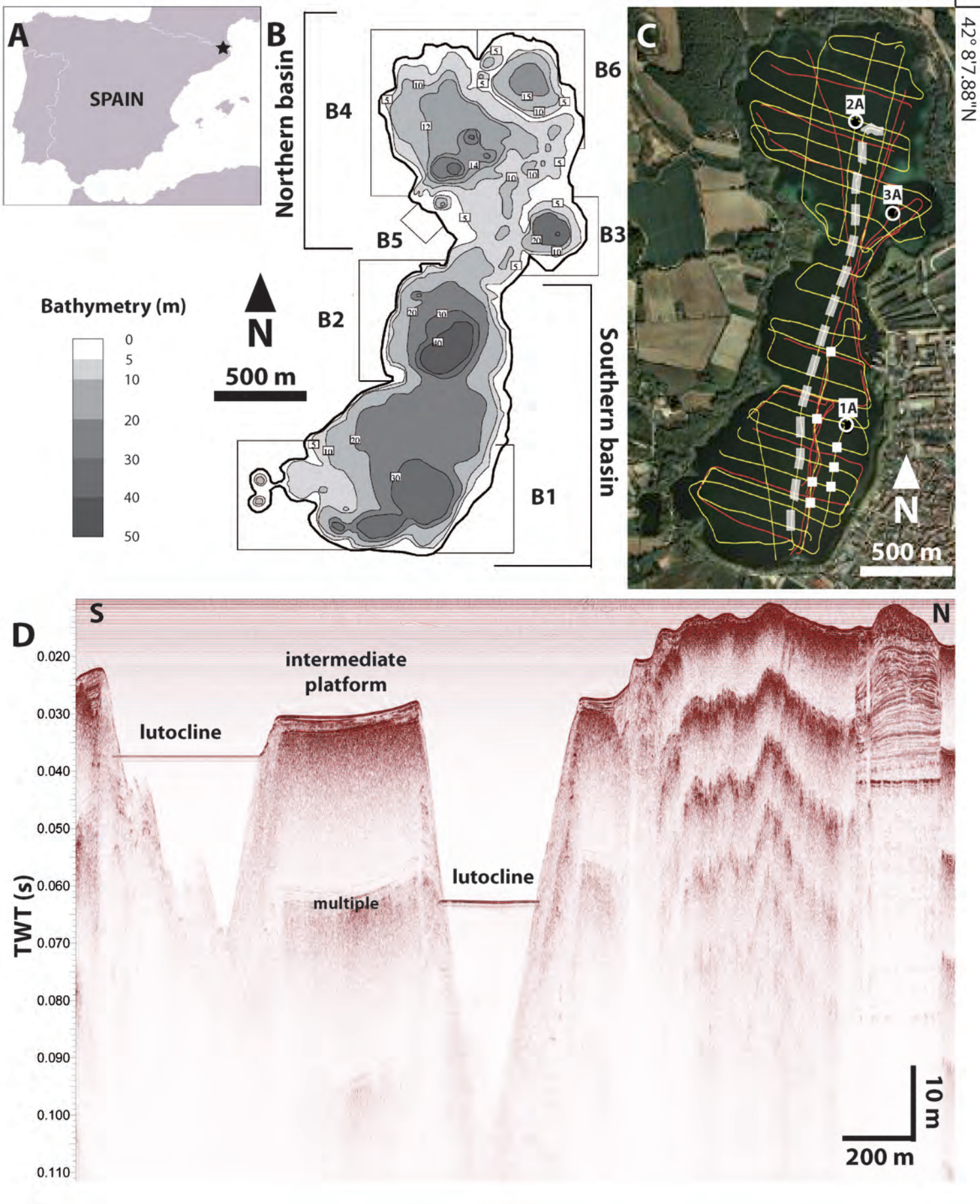
2°45'40.56"E
42° 8'7.88"N
A
SPAIN
B
Northern basin
Southern basin
B1
B2
B3
B4
B5
B6
Bathymetry (m)
0
5
10
20
30
40
50
N
500 m
C
2A
3A
1A
N
500 m
D
S
N
intermediate platform
lutocline
lutocline
multiple
TWT (s)
0.020
0.030
0.040
0.050
0.060
0.070
0.080
0.090
0.100
0.110
10 m
200 m

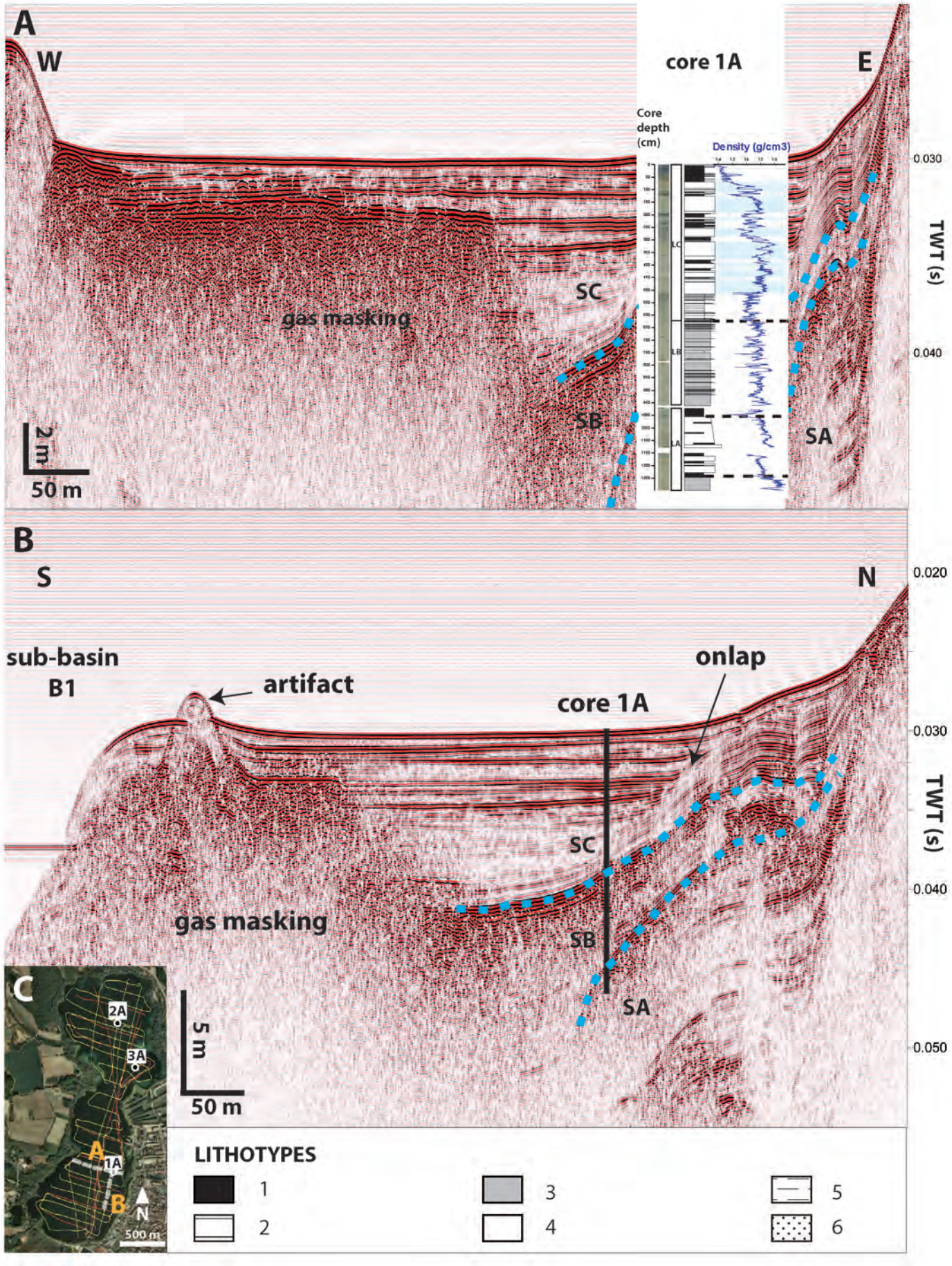
A
W
core 1A
E
Core depth (cm)
Density (g/cm3)
LC
LB
LA
SC
gas masking
SB
SA
2 m
50 m
0.030
0.040
TWT (s)
B
S
N
sub-basin B1
artifact
onlap
core 1A
SC
gas masking
SB
SA
5 m
50 m
0.020
0.030
0.040
0.050
TWT (s)
C
2A
3A
A
1A
B
N
500 m
LITHOTYPES
1
2
3
4
5
6

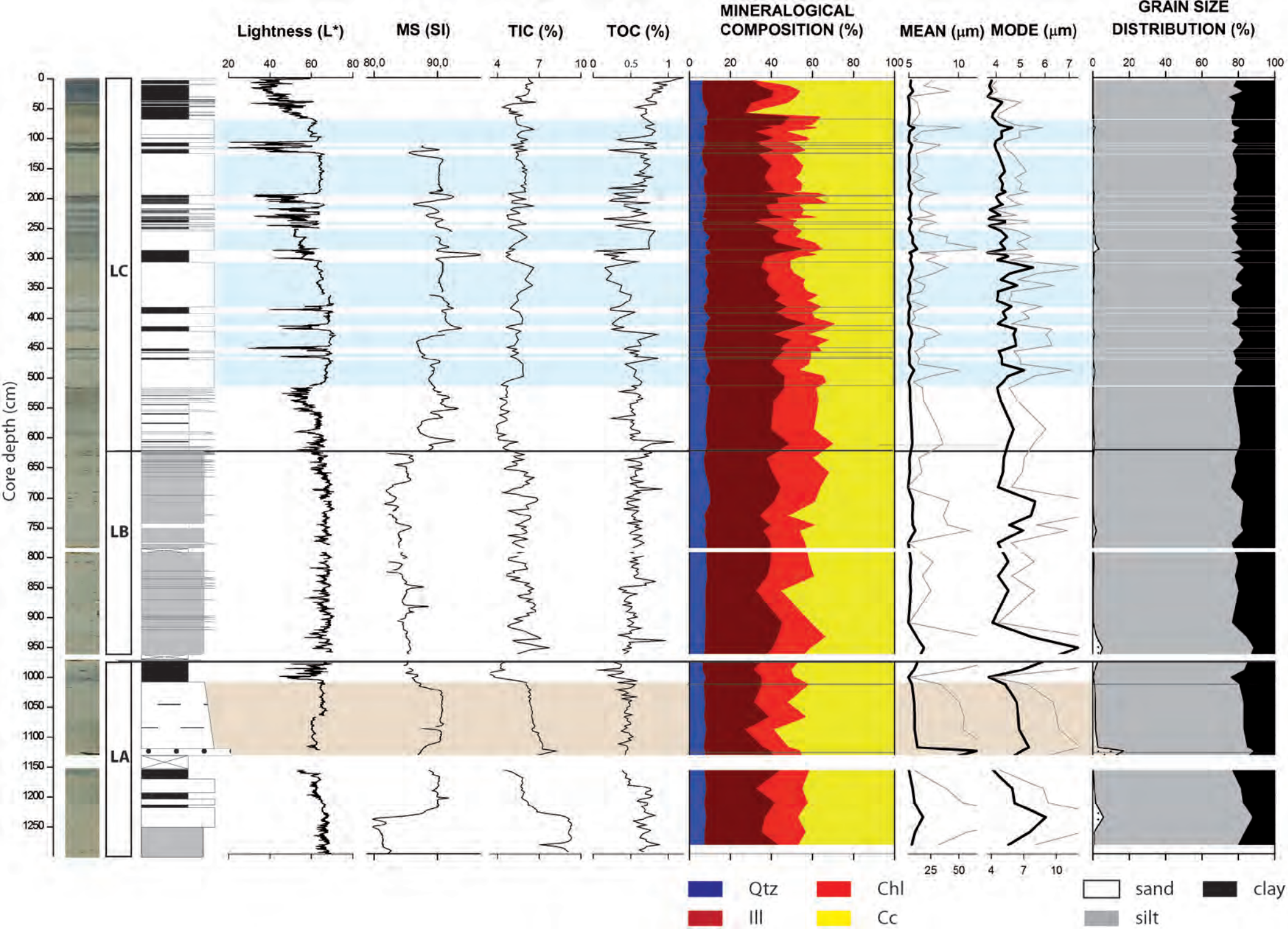
Lightness (L*)
MS (SI)
TIC (%)
TOC (%)
MINERALOGICAL COMPOSITION (%)
MEAN (μm)
MODE (μm)
GRAIN SIZE DISTRIBUTION (%)
Core depth (cm)
LC
LB
LA
Qtz
Chl
Ill
Cc
sand
clay
silt

A

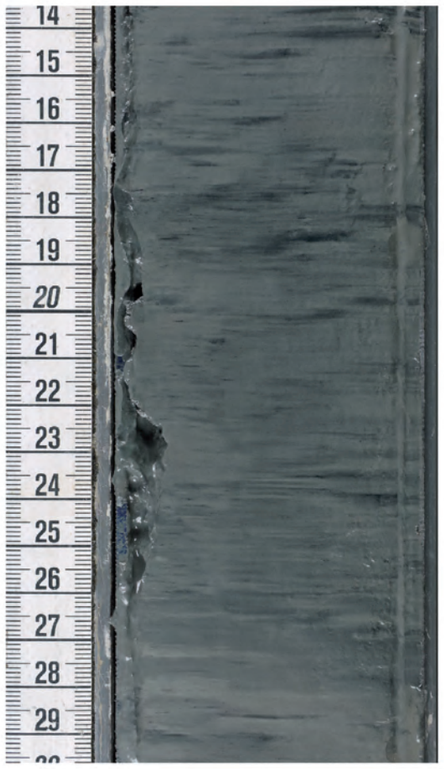

B

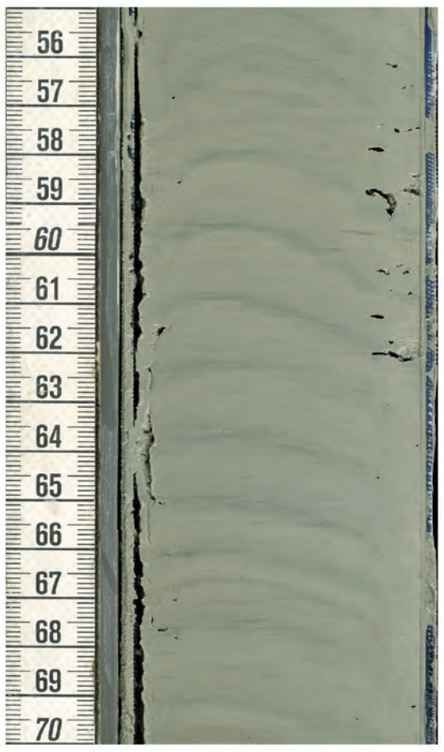

C

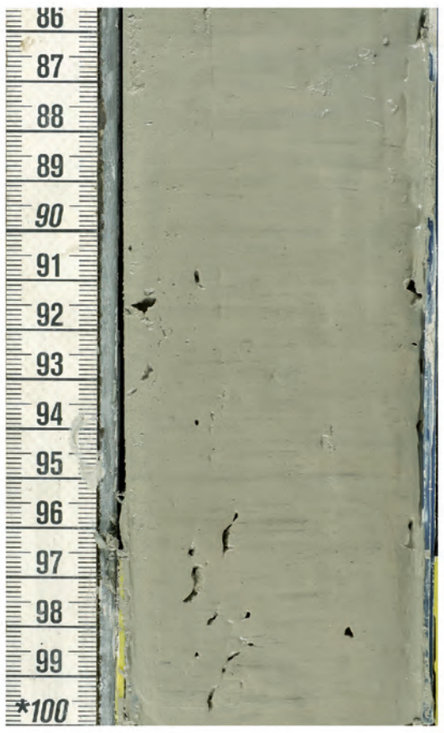

D

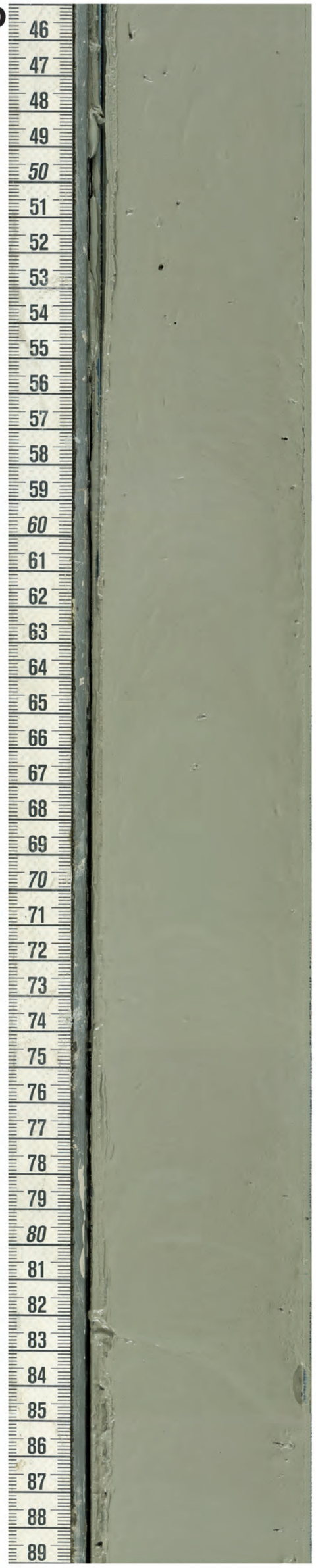

E

F

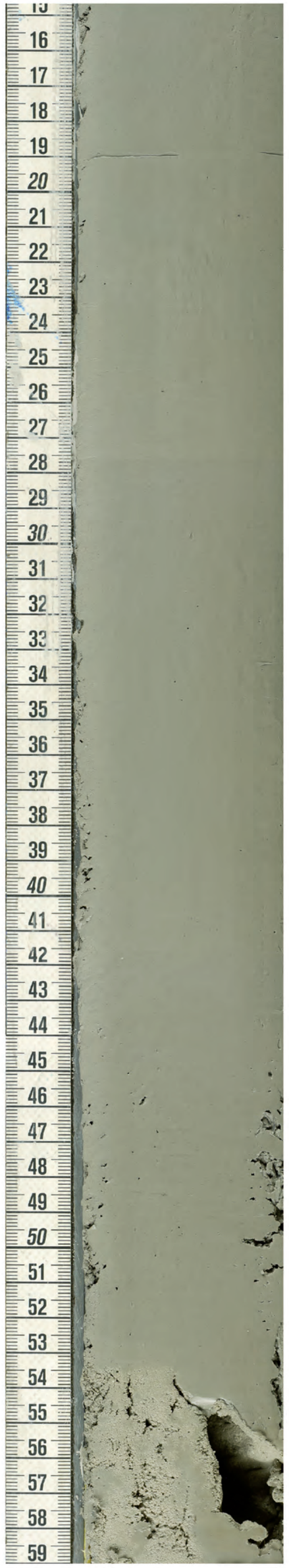

G

H

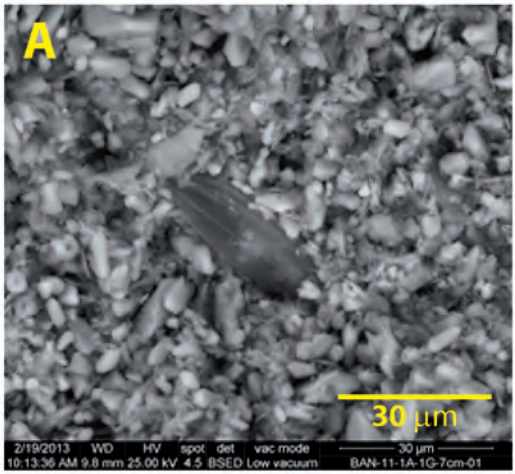
A
30 µm
2/19/2013 WD HV spot det vac mode 30 µm
10:13:36 AM 9.8 mm 25.00 kV 4.5 BSED Low vacuum BAN-11-1A-1G-7cm-01

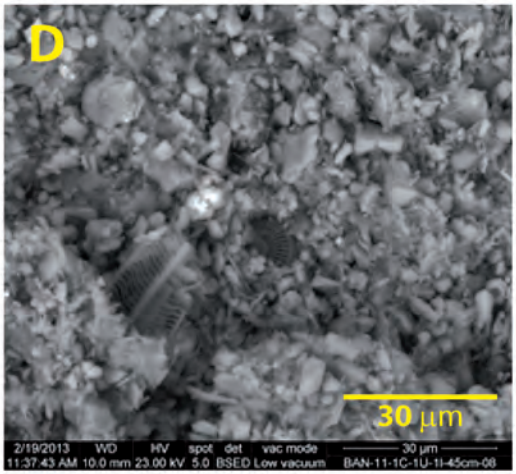
D
30 µm
2/19/2013 WD HV spot det vac mode 30 µm
11:37:43 AM 10.0 mm 23.00 kV 5.0 BSED Low vacuum BAN-11-1C-1U-1I-45cm-08

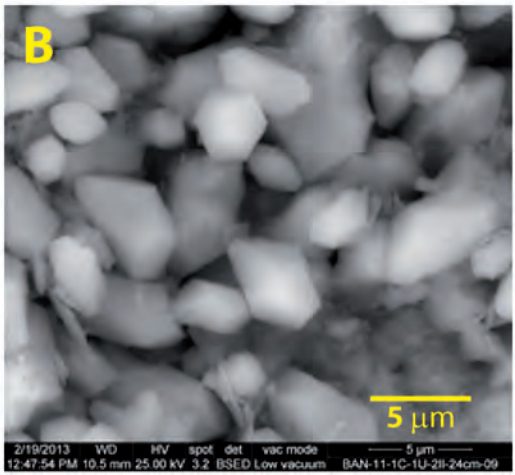
B
5 µm
2/19/2013 WD HV spot det vac mode 5 µm
12:47:54 PM 10.5 mm 25.00 kV 3.2 BSED Low vacuum BAN-11-1C-1U-2II-24cm-09

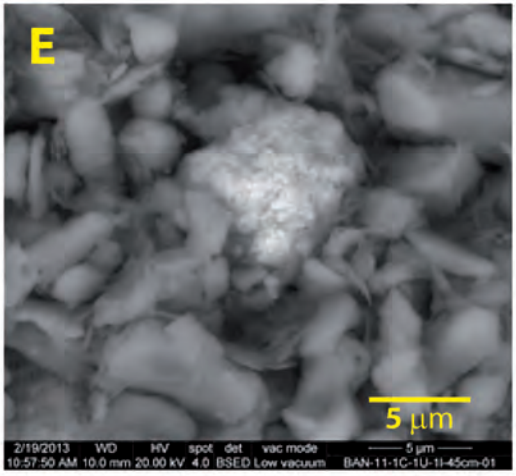
E
5 µm
2/19/2013 WD HV spot det vac mode 5 µm
10:57:50 AM 10.0 mm 20.00 kV 4.0 BSED Low vacuum BAN-11-1C-1U-1I-45cm-01

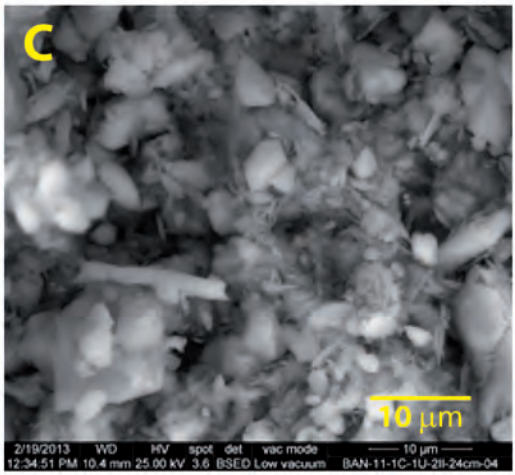
C
10 µm
2/19/2013 WD HV spot det vac mode 10 µm
12:34:51 PM 10.4 mm 25.00 kV 3.6 BSED Low vacuum BAN-11-1C-1U-2II-24cm-04

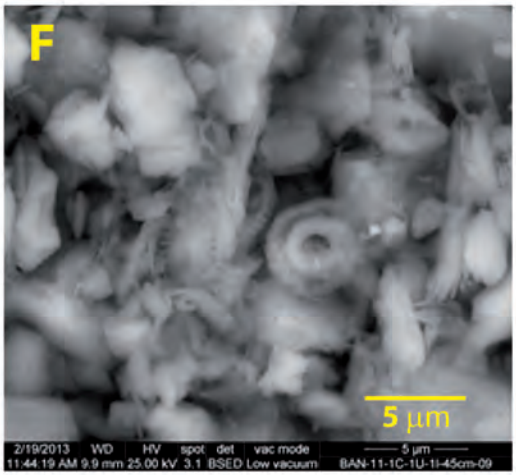
F
5 µm
2/19/2013 WD HV spot det vac mode 5 µm
11:44:19 AM 9.9 mm 25.00 kV 3.1 BSED Low vacuum BAN-11-1C-1U-1I-45cm-09

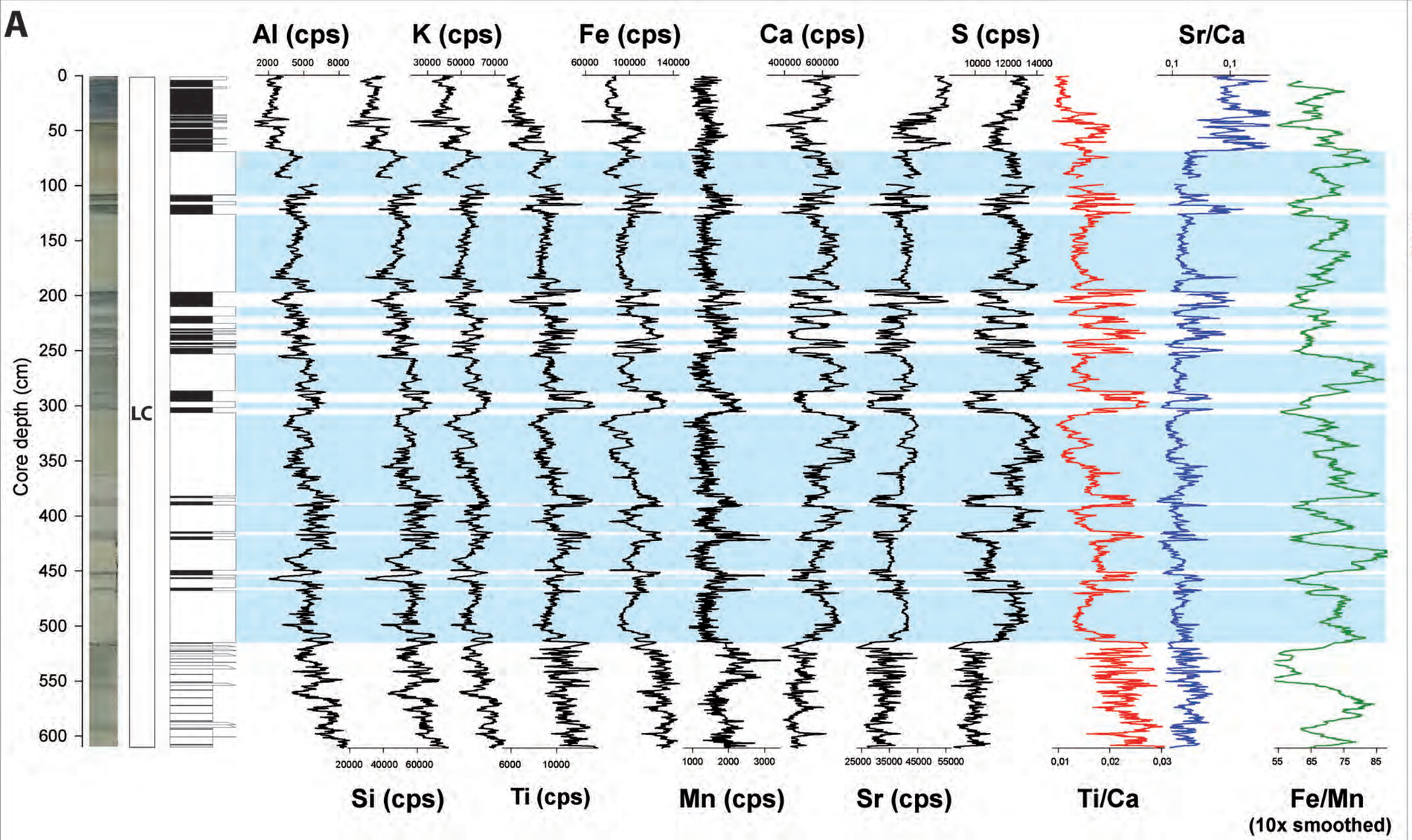
A
Al (cps)
K (cps)
Fe (cps)
Ca (cps)
S (cps)
Sr/Ca
Core depth (cm)
LC
Si (cps)
Ti (cps)
Mn (cps)
Sr (cps)
Ti/Ca
Fe/Mn
(10x smoothed)

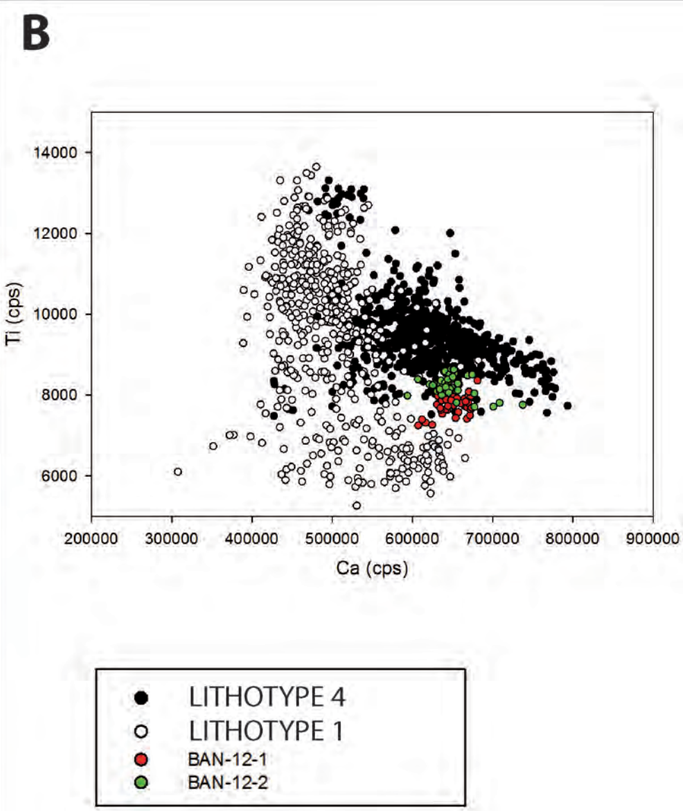
B
Ti (cps)
Ca (cps)
LITHOTYPE 4
LITHOTYPE 1
BAN-12-1
BAN-12-2

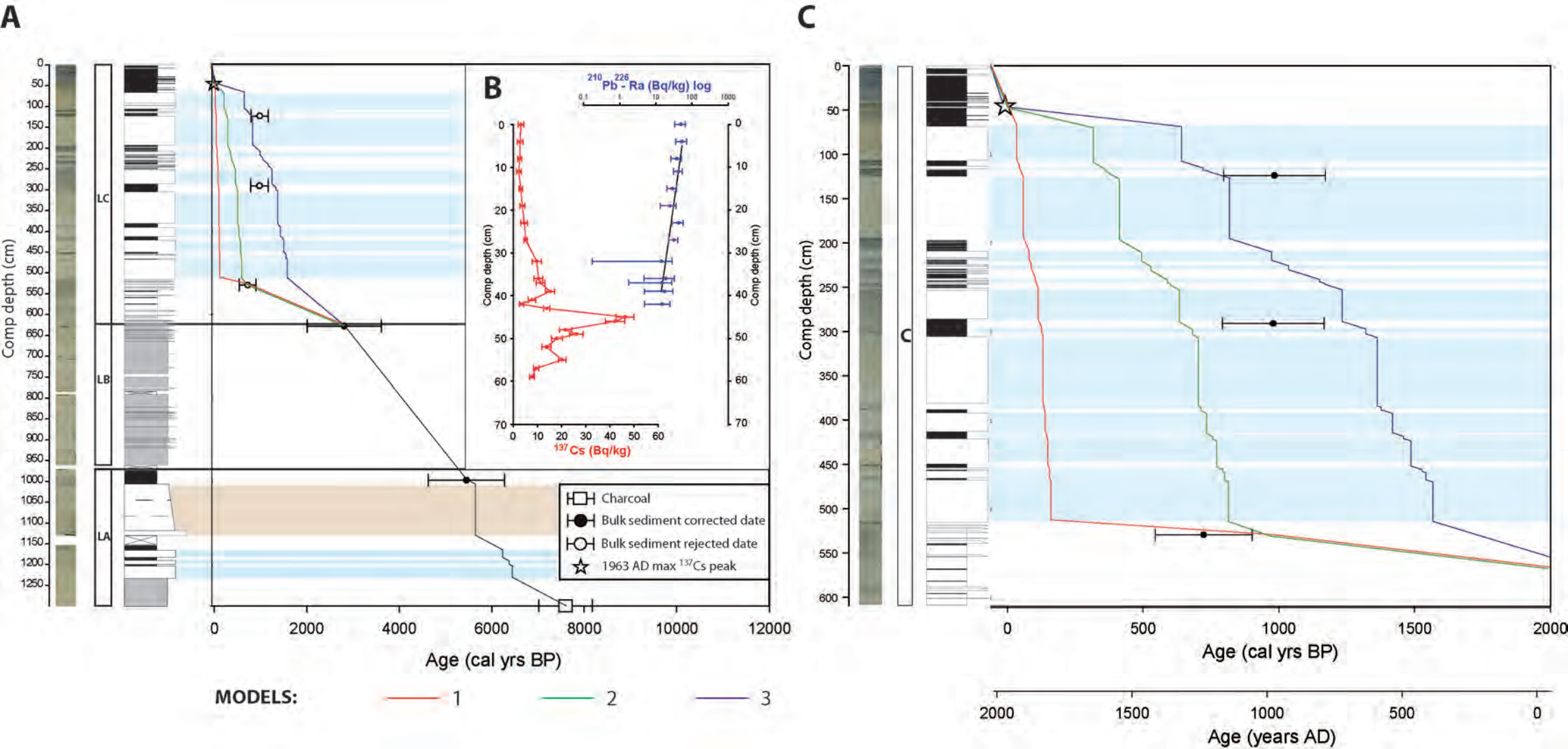
A
B
C
Comp depth (cm)
LC
LB
LA
^{210}Pb - ^{226}Ra (Bq/kg) log
^{137}Cs (Bq/kg)
Charcoal
Bulk sediment corrected date
Bulk sediment rejected date
1963 AD max ^{137}Cs peak
Age (cal yrs BP)
MODELS:
1
2
3
Age (years AD)

A

S

100 m

2 m

N

BAN-12-5 BAN-12-6 BAN-11-1A BAN-12-8

B1

B2

BAN-12-2 BAN-12-3 BAN-12-4

B

BAN-12-2
(suspended seds B1)

BAN-12-3 BAN-12-4 BAN-12-5 BAN-12-6 BAN-11-1A
(Master core)

BAN-12-8

BAN-12-1
(suspended seds B2)

10 cm

?

?

?

BAN-12-1

0.030

0.040

0.050

0.060

0.070

0.080

TWT (s)

C

2A

3A

1A

1

8

6

5

3

4

2

N

500 m